spontaneous ligand-independent internalization and the other that negatively regulates ligand-dependent CXCR4 internalization.

Materials and methods

Cells. The glioblastoma cell line NP2, human embryonic kidney (HEK) 293T, and HeLa, cells were maintained in RPMI-1640 (Sigma, Tokyo, Japan) supplemented with 10% FBS (Japan Bioserum, Tokyo, Japan), penicillin and streptomycin (Invitrogen, Tokyo, Japan). All cell lines were incubated at 37°C in the humidified 5% CO_2 atmosphere.

Plasmids. Full-length CXCR4 cDNA was amplified from a plasmid kindly provided by Dr Shioda[23] using the following primers: sense, 5′-ACCGGTGCCACCATGGAGGGGATCAGTATATACACTTCAG-3′, and antisense, 5′-AGATCTCGCTGGAGTGAAAACTTGAAGACTCAGACTC-3′. CXCR4 lacking the cytoplasmic tail (d-44) was amplified using the same sense primer and the antisense primer, 5′-AGATCTTGGCTCCAAGGAAAGCATAGAGGATGGG-3′. Polymerase chain reaction (PCR) fragments were cloned into the *Age* I-*Bgl* II sites of pEGFP-C2 (Clontech, Palo Alto, CA, USA) to create pCXCR4 FL and pCXCR4 d-44, respectively. To construct pCXCR4 FL- and d-44-GFP, the *Sna* BI-*Bgl* II fragments from pCXCR4 FL and d-44 were cloned into the *Sna* BI-*Bgl* II sites of pEGFP-N2, respectively (Clontech). To construct pCXCR4 FL- and d-44-GFP flag, the *Sna* BI-*Bgl* II fragments from pCXCR4 FL and d-44 were cloned into the *Sna* BI-*Bgl* II sites of pEGFP-flag in which the following annealed oligonucleotides had been inserted into the *Bsr* GI site of pEGFP-N2: forward, 5′-GTACGACTACAAAGACGATGACGACTATAAGTAAGC-3′, and reverse, 5′-GGCCGCTTACTTATAGTCGTCATCGTCTTTGTAGTC-3′. To construct pCMMP CXCR4 FL- and d-44-GFP, pCXCR4 FL- and d-44-GFP were digested with *Not* I, blunted using T4 DNA polymerase, and further digested with *Age* I. The Age *I*-blunted *Not* I fragments of both constructs were cloned into the pCMMP eGFP plasmid that had been digested with *Bam* HI, blunted with T4 DNA polymerase, and digested with *Age* I. pCMMP CXCR4 FL- and d-44-GFP-flag were constructed using the same strategy. CXCR4 deletion and point mutants were PCR-amplified using the sense primer 5′-ACCGGTGCCACCATGGAGGGGATCAGTGTGAAAACTTGAAGACTCAGACTC-3′ and the following reverse primers: d-6, 5′-AAGCTTGAGCTCGAGATCTCAGACTCAGACTCAGTGGAAAC-3′; d-10, 5′-AAGCTTGAGCTCGAGATCTCAGTGGAAACAGATGAATGTCC-3′; d-14, 5′-AAGCTTGAGCTCGAGATCTCTGAATGTCCACCTCGCTTTCC-3′; d-17, 5′-AAGCTTGAGCTCGAGATCTCACCTCGCTTTCCTTTGG-3′; d-22, 5′-AAGCTTGAGCTCGAGATCTCGGAGAGGATCTTGAGGCTGGACC-3′; d-31, 5′-AAGCTTGAGCTCGAGATCTCGCTCACAGAGGTGAGTGCGTGC-3′; E343A, 5′-CGAGATCTCGCTGGAGTGAAAACTTGAAGACTCAGACGCAGTGGAAACAGATGAATGTC-3′; S344A, 5′-CGAGATCTCGCTGGAGTGAAAACTTGAAGACTCAGCCTCAGTGGAAACAGATGAATGTC-3′; E345A, 5′-CGAGATCTCGCTGGAGTGAAAACTTGAAGACGCAGACTCAGTGGAAACAGATGAATGTC-3′; S346A, 5′-CGAGATCTCGCTGGAGTGAAAACTTGAAGCCTCAGACTCAGTGGAAACAGATGAATGTC-3′; S347E, 5′-CGAGATCTCGCTGGAGTGAAAACTTTCAGACTCAGACTCAGTGGAAACAGATGAATGTC-3′; H350E, 5′-CGAGATCTCGCTGGACTCAAAACTTGAAGACTCAGACTCAGTGGAAACAGATGAATGTC-3′; S347E/H350E, 5′-CGAGATCTCGCTGGACTCAAAACTTTCAGACTCAGACTCAGTGGAAACAGATGAATGTC-3′; and E343/345D, 5′-CGAGATCTCGCTGGAGTGAAAACTTGAAGAGTCAGAGTCAGTGGAAACAGATGAATGTC-3′. The PCR fragments were cloned into the *Age* I-*Bgl* II sites of pCMMP CXCR4 FL-GFP-flag, replacing wild-type with mutant CXCR4. Protein expression of each mutant in 293T cells was verified by Western blot analysis.

Immunoblotting. Immunoblotting was performed as described.[24,25] The primary antibody was anti-green fluorescent protein (GFP) polyclonal antibody (Beckton Dickinson, San Jose, CA, USA). The secondary probe was EnVision+ (Dako, Glostrup, Denmark). Signals were visualized with an LAS3000 imager (Fuji Film, Tokyo, Japan) after treating the membranes with the Lumi-Light Western Blotting Substrate (Roche Diagnostics GmbH, Mannheim, Germany).

Flow cytometry. Cells were labeled with anti-CXCR4 antibodies recognizing the N-terminus conjugated with R-phycoerythrin (PE; 2B11, BD Pharmingen, San Diego, CA) or recognizing the second extracellular loop (12G5) conjugated with either PE or PE-Cy5 (Beckton Dickinson) for 30 min at 4°C. Cells were washed once with phosphate-buffered saline (PBS) supplemented with 1% FBS and analyzed by FACS Aria (Beckton Dickinson). To isolate GFP-expressing NP2 cells, cells were infected with murine leukemia virus (MLV)-based retroviral vectors as described.[25] Cells exhibiting similar green fluorescence intensities were gated and sorted by FACS Aria. Efficiency of internalization was measured by comparing mean fluorescence intensities for cell surface CXCR4 detected by a PE-labeled 2B11 monoclonal antibody before and after SDF-1α treatment (200 ng/mL, Peprotech EC, London, UK).

Microscopic analysis and imaging of cells. To judge a phenotype of a CXCR4 mutant, three independent scientists investigated the mutant cell phenotype under a fluorescent microscope (Olympus, Tokyo, Japan). Each scientist investigated more than 1000 cells for each mutant. More than 99% of cells of a mutant fell in the indicated phenotypic category. These phenotypes were unchanged for more than a year of continuous cultivation in tissue culture. For imaging, NP2 cells were grown on glass plates for more than 24 h, fixed in 4% formaldehyde in PBS for 5 min, stained with Hoechst 33258, mounted (Vectorshield, Vector Laboratories, Burlingame, CA, USA), and imaged using a confocal microscope META 510 (Carl Zeiss, Tokyo, Japan). A representative cell for each CXCR4 mutant carrying a wide cytoplasm was chosen such that the spatial resolution was high. The focal plane just above the glass surface was scanned with an optical thickness of approximately 1 μm. For the imaging of subcellular compartments, cells were incubated with either BODIPY TR ceramid, ER-Tracker Blue-White DPX, or Lysotracker Red DND-99 (Invitrogen) according to the manufacturer's protocol and imaged without fixation. Image brightness and contrast were processed by META510 software (Carl Zeiss). Unless noted, cells were imaged at ×630 magnification, the GFP signal was displayed in green, and Hoechst 33258-stained nuclei were blue. To visualize ligand-induced internalization, cells were treated with 200 ng/mL SDF-1α before fixation. The live cell imaging was performed using Leica DFC350FX system and the images were processed by FW4000 software (Leica Microsystems, Tokyo, Japan). Cells were plated on the glass-bottomed dish (Matsunami glass, Kishiwada, Japan) and incubated at 37°C in the humidified 5% CO_2 atmosphere during the monitoring.

Cell migration assay. Cell migration was measured using an HTS FluoroBlok Multiwell Insert System (8.0 μm pore size, BD Falcon) according to the manufacturer's protocol. For stimulation assays, cells were incubated without serum overnight before SDF-1α treatment (200 ng/mL). Cells were allowed to migrate overnight.

Statistical analysis. Significance of differences were determined by a Student's *t*-test. *P*-values less than 0.05 were considered significant.

RESULTS

Deleting 10 amino acids from the carboxyl end of CXCR4 alters the efficiency of constitutive internalization. Previous studies indicated that the cytoplasmic tail of CXCR4 amino acids 308–352 plays

doi: 10.1111/j.1349-7006.2007.00388.x

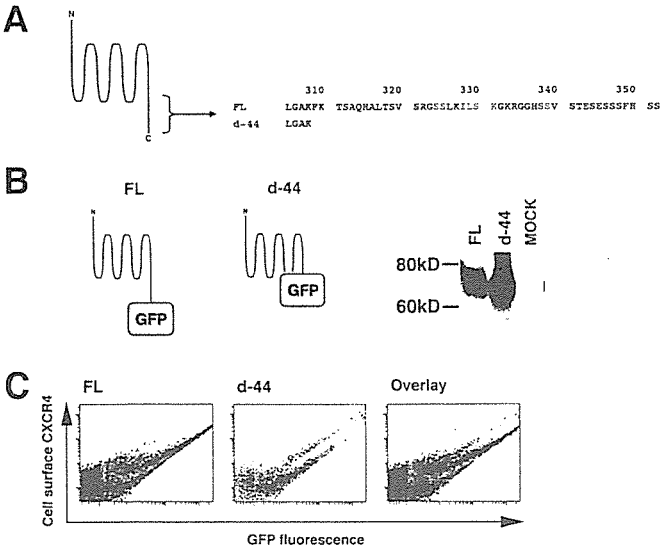

Fig. 1. The effect of stromal cell-derived factor-1 alpha (SDF-1α) treatment on NP2 cells expressing CXCR4 mutants. (a) Cells expressing d-17 were treated with SDF-1α, incubated at 37°C for the indicated times, fixed and imaged. The blue signal represents the Hoechst-stained nucleus. (Original magnification, ×630; bar, 10 μm). (b) FACS analysis to measure internalization efficiency of cell surface CXCR4 and mutant forms 2 h after SDF-1α exposure. The average and standard deviation from the indicated number of independent experiments are shown. Asterisks represent statistically significant difference from the FL levels ($P < 0.01$). (c) Cell migration assay to assess response of cells expressing CXCR4 and mutants to SDF-1α. The number of migrated cells in three to six randomly selected fields was counted and the average and standard deviation were calculated. (□) number of migrated cells in the absence of ligand; (■) migration in the presence of ligand. (*) statistically significant differences in the number of migrated cells between SDF-1α-untreated and -treated cells ($P < 0.01$).

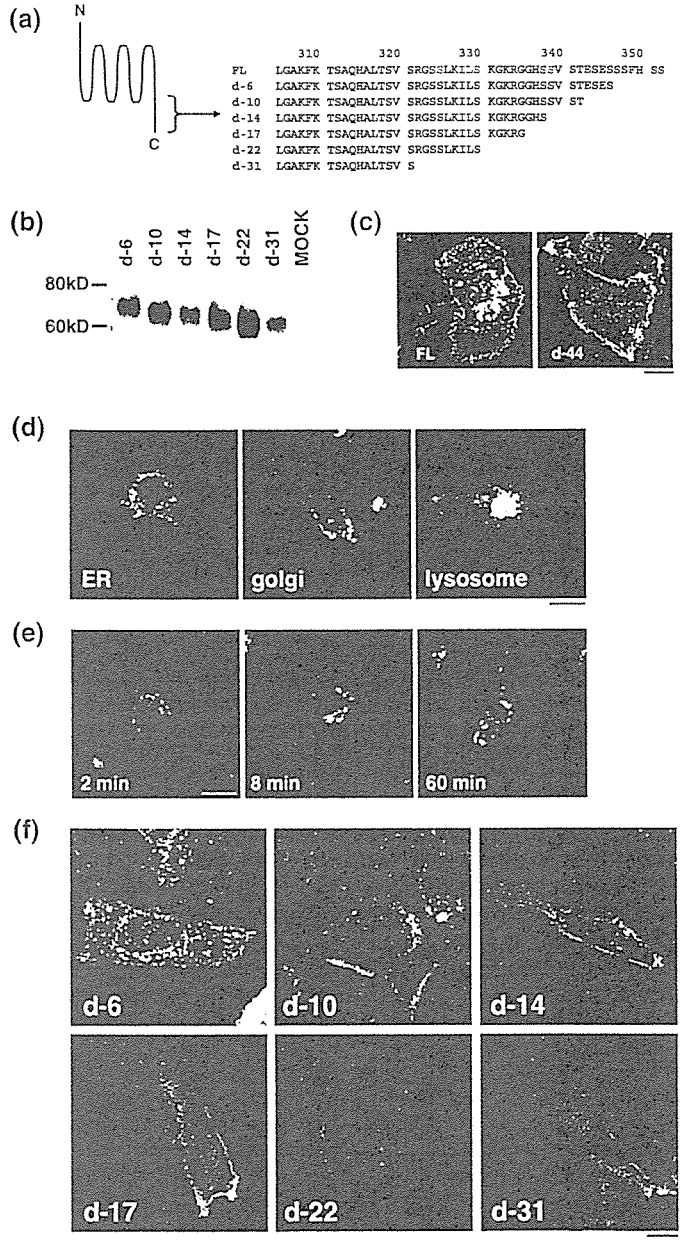

Fig. 2. Expression profiles of CXCR4 and a mutant with cytoplasmic tail deletion. (a) Schematic representation of CXCR4. The N-terminus CXCR4 is exposed in the extracellular space and the C-terminus is intracellular. Gray represents the lipid bilayer. The amino acid sequence of the cytoplasmic tail is shown. Residues in red are required for ligand-induced endocytosis. The CXCR4 d-44 mutant lacks amino acid 309–351. (b) Schematic representation and Western blot of FL and d-44 constructs. (c) Flow cytometry profiles of FL and d-44 expressed in 293T cells. The horizontal axis represents green fluorescence intensity indicative of green fluorescent protein (GFP)-tagged CXCR4 protein levels, and the vertical axis is PE-Cy5 fluorescence intensity, reflecting cell surface CXCR4 detected by the anti-CXCR4 antibody. GFP-positive cells expressing FL are colored in red (left) and those expressing d-44 in green (middle). The expressional differences between FL and d-44 is highlighted on the overlay plot (right).

a critical role in ligand-dependent internalization (Fig. 1a). Also, it has been shown in transfected cells that cell surface levels of CXCR4 lacking the cytoplasmic tail (equivalent to the d-44 mutant here) are higher than those of the full length, wild-type protein (hereafter designated FL), suggesting that the cytoplasmic tail of CXCR4 regulates steady-state internalization.[26,27] To confirm this, we constructed expression plasmids of CXCR4 FL and d-44 fused to GFP or GFP-FLAG at the C-terminus. Previous studies and data reported here indicated that CXCR4 function is not affected by this modification.[28] The expression of each construct was verified by Western blot analysis (Fig. 1b). Single cell-based quantitative analyzes revealed that the ratio of cell surface levels to the total amount of CXCR4 FL (Fig. 1c, left) was consistently lower than that of d-44 (Fig. 1c, middle) at any expression levels (Fig. 1c, right for the comparison). These data supported previous findings and demonstrate that constitutive internalization occurs at any level of CXCR4 expression.

To further examine the contribution of the cytoplasmic tail to post-translational trafficking of CXCR4, we devised a system utilizing the human NP2 glioma line: NP2 cells are flat and exhibit a large cytoplasmic space such that intracellular compartments can be well resolved under the microscope. NP2 cells also lack endogenous CXCR4[29] and SDF-1α (data not shown), both of which could potentially affect distribution of transduced CXCR4. However, NP2 cells are capable of appropriate signaling in response to CXCR4/SDF-1α interaction. We generated a series of CXCR4 deletion mutants lacking the cytoplasmic tail (Fig. 2a) and transduced them into NP2 cells using MLV vectors. Cells bearing similar green fluorescence intensities were collected by FACS sorter. The expression of each mutant was verified by Western blot analysis (Fig. 2b). Microscopic observations revealed that cells expressing FL were bordered by green fluorescence, and significant green fluorescence was detected in vesicular compartments of varying diameters lying close to the nucleus surrounding the nucleus (hereafter designated the FL phenotype, Fig. 2c, left). Vesicles around the nucleus were

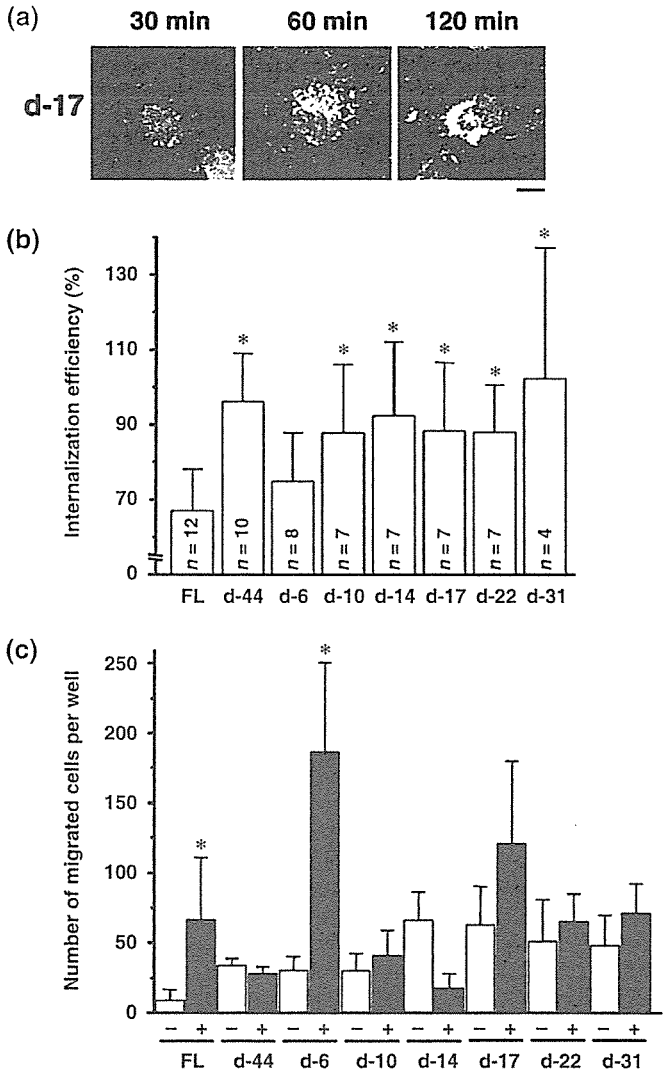

Fig. 3. Identification of the amino acids required for steady-state CXCR4 internalization. (a) Amino acid sequences of the cytoplasmic tail of FL and deletion mutants. Residues in red are required for ligand-induced endocytosis. (b) The protein expression of each mutant in 293T cells was verified by Western blot analysis. (c) Confocal micrographs of NP2 cells expressing FL and d-44 mutant proteins. The blue signal represents the Hoechst-stained nucleus. (Original magnification, ×630; bar, 10 μm.) (d) Confocal micrographs showing NP2 cells expressing CXCR4 FL stained with ER, Golgi, or lysosome organella markers. The organella marker signal is shown in red, the GFP signal is in green. The pixels that both red and green signals co-localized are shown in yellow. (Original magnification, ×630; bar, 10 μm.) (e) CXCR4 FL trafficking in the absence of SDF-1α in NP2 cells. Cell surface CXCR4 FL was labeled with an antibody conjugated with PE-Cy5 (red), incubated at 37°C for the indicated times, fixed and imaged. (Original magnification, ×630; bar, 10 μm.) (f) Confocal micrographs of NP2 cells expressing FL and mutant proteins. The intracellular vesicular green fluorescence reflecting steady-state internalization can be seen in the d-6 mutant. The blue signal represents the Hoechst-stained nucleus. (Original magnification, ×630; bar, 10 μm.)

mostly lysosomes, as demonstrated by fluorescent organella marker analyses in which cells expressing CXCR4 FL-GFP stained with the lysosomal marker yielded a substantial amount of co-localization signal. On the other hand, only a mall amount of co-localization signal was detected when the ER or Golgi markers were used (Fig. 2d), consistent with our biochemical fractionation (unpublished data) and previous publications.[16,27,28,30] The active constitutive internalization was visualized by labeling cell surface CXCR4 by PE-Cy5-conjugated monoclonal antibody followed by fluorescence imaging after cells were incubated at 37°C (Fig. 2e). The live cell imaging revealed that internalizing GFP-positive vesicles trafficked at an average velocity of 4.7 mm/h ($n = 15$), which is within the range of clathrin-dependent vesicular transport (2–20 mm/h), not that of caveolin-dependent vesicular transport (25–170 mm/h).[31–35] These data suggest that the FL is constitutively internalized from the cell surface to the cytoplasmic compartment. In sharp contrast, most green fluorescent signals from d-44 mutant-expressing cells were detected at the cell surface, and only a few small GFP-positive vesicles were seen in the cytoplasm near the nucleus (hereafter designated the d-44 phenotype, Fig. 2c, right). Similar observations were made in d-10, d-14, d-17, d-22 and d-31 mutant-expressing cells (Fig. 2f). The d-6 construct displayed a phenotype similar to FL, although the intracellular GFP signal was less prominent (Fig. 2c). Similar results were obtained in HeLa and 293 cells (data not shown). These data suggest that wild-type CXCR4 was trafficked to the plasma membrane but was internalized spontaneously. Thus, steady-state internalization appeared to be regulated by amino acids located between d-6 and d-10 (e.g. amino acids 343–346).

Steady-state and SDF-1α-induced CXCR4 internalization is genetically separable. Next, we investigated distribution of CXCR4 protein and cell migration after SDF-1α treatment. Confocal analysis showed that after SDF-1α exposure, cells expressing FL, d-6 and d-17 mutants showed GFP signals in intracellular compartments, which were enhanced 60 min after SDF-1α treatment, an effect most clearly shown in d-17-expressing cells (Fig. 3a). GFP signals from intracellular vesicles gradually disappeared 1–2 h after exposure to ligand. Such redistribution of GFP signals was not observed in cells expressing d-10, d-14, d-22, d-31 and d-44 (data not shown). Cell surface levels of CXCR4 before and after SDF-1α treatment were measured by FACS analysis undertaken with an antibody directed against the CXCR4 N-terminus, because that antibody did not interfere with ligand–receptor interaction (Fig. 3b). The downregulation of cell surface levels of FL 2 h after ligand exposure was 67.1 ± 11.1%, whereas that of d-44 was 96.3 ± 12.3% (average and standard deviation from 12 and 10 independent experiments, respectively), consistent with previous reports.[17,27,28] Ligand-induced downregulation of d-6 was 74.9 ± 12.9% ($n = 8$), similar to FL levels. Ligand-induced internalization was significantly less efficient in cells expressing d-10, d-14, d-17, d-22, d-31 and d-44 mutants when compared with FL ($P < 0.001$). Although the d-17 mutant supported ligand-facilitated internalization, as evidenced by microscopic observation, cell surface levels remained unchanged (Fig. 3a,b). This may be due in part to rapid recruitment of newly synthesized d-17 to the cell surface.

Next, we examined cells expressing CXCR4 mutants in response to SDF-1α. Migration results from intracellular signaling initiated by SDF-1α/CXCR4 interaction. Induction of cell migration by SDF-1α in cells expressing FL was 7.2-fold that of untreated cells ($P < 0.05$). In contrast, migration of cells expressing d-44 in response to SDF-1α was undetectable. These data are in agreement with a previous report.[26] The d-6 mutant, which is internalized upon SDF-1α treatment, supported ligand-promoted cell migration by 6.1-fold ($P < 0.01$) relative to untreated cells, similar to FL. Other deletion mutants tested did not display enhanced cell migration following ligand treatment, except for d-17, which showed modestly enhanced (1.9-fold) migration relative to untreated cells, which was not statistically significant. When basal migratory activities were compared, removal of six or more amino acids from the cytoplasmic tail appeared to potentiate migration in the absence of ligand (open bars, Fig. 3c). These data suggest that constitutive internalization is regulated independently of ligand-facilitated internalization.

Identification of CXCR4 S(E/D)S as a ligand-independent internalization motif. The above data indicated that the carboxy-terminal four

doi: 10.1111/j.1349-7006.2007.00388.x

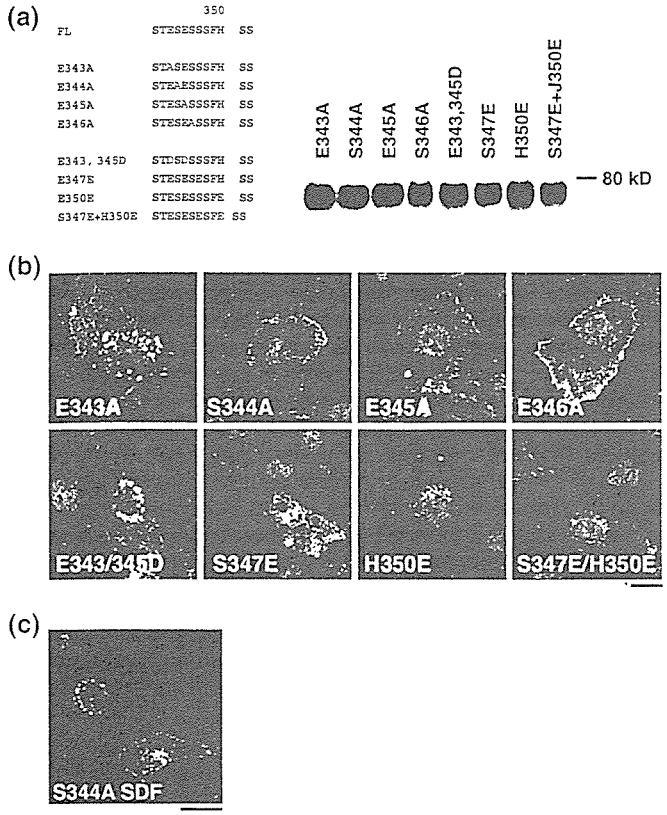

Fig. 4. Characterization of the SDF-1α-independent internalization motif of CXCR4. (a) Left, amino acid sequences of CXCR4 FL and substitution mutants. Letters in red indicate introduced mutations. Right, protein expression of each mutant in 293T cells was verified by Western blot analysis. (b) Confocal micrographs of NP2 cells expressing each mutant. The blue signal represents the Hoechst-stained nucleus. (Original magnification, ×630; bar, 10 μm.) (c) NP2 cells expressing the S344A mutant treated with SDF-1α for 2 h are shown. The blue signal represents the Hoechst-stained nucleus. (Original magnification, ×630; bar, 10 μm.)

amino acids (ESES; residues 343–346) likely function in ligand-independent CXCR4 internalization. To further characterize which amino acids are required for ligand-independent internalization, we generated alanine substitution mutants for each of the four amino acids in the context of FL and examined their phenotypes (Fig. 4a). Protein expression of mutants was verified in Western blot analysis (Fig. 4a). Among the four mutants, the E343A mutant showed the FL phenotype, while the others displayed the d-44 phenotype in the absence of ligand (Fig. 4b). These data demonstrate that Ser^{344}-Glu^{345}-Ser^{346} constitute the core motif for SDF-1α-independent CXCR4 internalization. Both E345A and S346A mutants exhibited the Thr^{342}-Glu^{343}-Ser^{344} sequence adjacent to the original SES sequence. However, this 'SES-like' motif did not support constitutive internalization, suggesting that Thr cannot substitute for Ser to maintain functionality as a constitutive internalization motif. We reasoned that if such a motif requires an acidic amino acid between two serine residues, changing Glu to Asp should maintain the motif's function. Thus, we constructed a mutant in which Glu was replaced with Asp (E343/345D; Fig. 4a). Also, to determine whether two adjacent SES sequences could augment the FL phenotype, we substituted Ser^{347} with Glu (S347E), creating an additional SES motif next to the original SES one (Fig. 4a). As controls, we created H350E and S347E/H350E mutants (Fig. 4a). Expression of these mutants was verified by Western blot analysis (Fig. 4a). Interestingly, the E343/345D mutant retained the FL phenotype (Fig. 4b), indicating that an acidic residue is required to maintain function of the constitutive internalization motif. S347E showed an intermediate phenotype in which numerous fine GFP-positive vesicles were seen close to the nucleus (Fig. 4b). These data indicate that the two adjacent SES sequences do not augment the FL phenotype but actually interfere with steady-state internalization. Both H350E and S347E/H350E mutants also showed an intermediate phenotype (Fig. 4b), suggesting that more than three acidic amino acids close to the SES motif may inhibit its function, potentially by generating a negative charge cluster. Overall, we conclude that the SDF-1α-independent internalization motif is located at amino acids 344–346 of the CXCR4 cytoplasmic tail.

Finally, we analyzed phenotypes of the S344A mutant in greater detail. Two hours after SDF-1α treatment, cells expressing this mutant showed accumulation of GFP signals at perinuclear regions, similar to the d-17 mutant (Figs. 1a and 4c). FACS analysis revealed that cell surface levels of S344A decreased to $70.8 \pm 11.7\%$ ($n = 7$) following SDF-1α treatment relative to untreated cells, almost as efficient as FL (Fig. 3b). Migratory activity of cells expressing the S344A mutant was stimulated 3.0-fold by SDF-1α, while that of cells expressing FL assayed in parallel showed a 5.8-fold increase relative to untreated cells. These data demonstrate that the S344A mutant, which is defective in constitutive internalization, can undergo ligand-dependent internalization and stimulate migration. Along with the d-17 data, our observations strongly suggest that genetic elements required for the ligand-dependent and -independent internalization are separable.

Discussion

We demonstrated here that CXCR4 is constitutively internalized in the absence of SDF-1α and that steady-state trafficking of CXCR4 is regulated by its cytoplasmic tail. We show that the three amino acid motif, Ser^{344}-Glu^{345}-Ser^{346}, within the cytoplasmic tail is essential for efficient steady-state internalization of CXCR4. Our work indicates that ligand-independent internalization of CXCR4 is genetically separable from ligand-dependent internalization: mutants defective in steady-state internalization (d-17 and S344A) were competent to respond to SDF-1α-promoted internalization signals. That residues required for ligand-dependent endocytosis (Ser324, 325, 330, 338, 339, Ile^{328} Leu^{329} and Lys^{331}; summarized in Fig. 1a)[16–18] do not overlap with those required for ligand-independent internalization, further supports the idea that these activities are separable.

Interestingly, the d-17 mutant displayed SDF-1α-promoted internalization, whereas the d-14 and d-22 mutants did not. These data suggest that an element between amino acids 336 and 342 negatively regulates ligand-initiated CXCR4 internalization. We are currently determining what amino acids are required for that motif. What is unique about the constitutive internalization motif is its position effect in terms of the distance of the motif from the "body" of the receptor. SES-like motifs can be found in the cytoplasmic tails of both CXC-chemokine receptors (for example, CXCR3) and CC-chemokine receptors including CCR2, CCR5 and CCR7. Indeed, these receptors share similar amino acid sequences in which two acidic amino acids (mostly Asp) positioned between the 36th and 45th amino acids of the cytoplasmic tail, where Ser and Thr residues are often in the close proximity to the acidic amino acids but positively charged amino acids, are infrequent. We hypothesize that for the ligand-independent internalization motif to function, the SES motif or its equivalent must be positioned at approximately the 40th residue of the cytoplasmic tail.

Many GPCR, including α1a-adrenoceptor, and the μ-opioid receptor, are spontaneously internalized.[36,37] Therefore, we conclude that various GPCR actively and continuously undergo endocytosis in the absence of ligand in a manner similar to

CXCR4 and hypothesize that the function of constitutive receptor internalization is to fine-tune the threshold at which cells sense ligand. Cells should be able to rapidly post up- and downregulate cell surface levels of CXCR4 using post-translational mechanisms. Such regulation should enable cells to migrate toward SDF-1α-rich tissues as needed and should also prevent inappropriate cells from migrating.

Our work is relevant to cancer cell metastasis and the pathogenesis of WHIM syndrome. Cell surface levels of CXCR4 positively correlate with cancer cells' ability to metastasize.[5,19] We hypothesize that enhanced metastatic capabilities of cancer cells could be due in part to mutations that disrupt the function of SES motif, which would result in upregulation of cell surface levels of signal-competent CXCR4 (as exemplified by the E344A mutant). As for WHIM syndrome, it was recently reported that it is due to mutations within CXCR4's cytoplasmic domain.[14,38] Interestingly, these mutations result in loss of SES motif. We predict that loss of the SES motif should increase cell surface CXCR4 levels. Although CXCR4 mutations generated here are not identical to reported WHIM mutations, the d-10 mutant resembles mutations seen in WHIM syndrome, and it exhibits enhanced basal cell migratory activity. Increased cell surface CXCR4 or increased migratory potential may contribute to WHIM pathogenesis. The response of d-10-expressing cells to SDF-1α, however, was not as robust as that of cells derived from WHIM.[39,40] This discordance may be partly due to the cell type differences, as we have employed a glioblastoma cell line for our studies.

Thus, CXCR4 is a potentially important therapeutic target not only for cancers but for other conditions such as HIV-1 infection, chronic autoimmune disease, and genetic disorders including WHIM syndrome. CXCR4 also plays critical roles in embryogenesis, homeostasis and inflammation. Although there are potential caveats for treating cancer with CXCR4 antagonists, our data furthers the understanding of mechanisms regulating CXCR4 and could be useful in devising therapeutic strategies.

Acknowledgments

We thank Drs Toshitada Takemori and Tsutomu Murakami for critical reading of the manuscript. This work was supported in part by the Japan Human Science Foundation, the Japanese Ministry of Health, Labor and Welfare, and the Japanese Ministry of Education, Culture, Sports, Science and Technology.

References

1 Gether U. Uncovering molecular mechanisms involved in activation of G protein-coupled receptors. *Endocr Rev* 2000; **21**: 90–113.
2 Ferguson SS. Evolving concepts in G protein-coupled receptor endocytosis: the role in receptor desensitization and signaling. *Pharmacol Rev* 2001; **53**: 1–24.
3 Sapede D, Rossel M, Dambly-Chaudiere C, Ghysen A. Role of SDF1 chemokine in the development of lateral line efferent and facial motor neurons. *Proc Natl Acad Sci USA* 2005; **102**: 1714–8. Epub 2005 January 19.
4 Coughlan CM, McManus CM *et al.* Expression of multiple functional chemokine receptors and monocyte chemoattractant protein-1 in human neurons. *Neuroscience* 2000; **97**: 591–600.
5 Muller A, Homey B, Soto H *et al.* Involvement of chemokine receptors in breast cancer metastasis. *Nature* 2001; **410**: 50–6.
6 Zou YR, Kottmann AH, Kuroda M, Taniuchi I, Littman DR. Function of the chemokine receptor CXCR4 in haematopoiesis and in cerebellar development. *Nature* 1998; **393**: 595–9.
7 Ma Q, Jones D, Borghesani PR *et al.* Impaired B-lymphopoiesis, myelopoiesis, and derailed cerebellar neuron migration in CXCR4- and SDF-1-deficient mice. *Proc Natl Acad Sci USA* 1998; **95**: 9448–53.
8 Wang JF, Park IW, Groopman JE. Stromal cell-derived factor-1alpha stimulates tyrosine phosphorylation of multiple focal adhesion proteins and induces migration of hematopoietic progenitor cells: roles of phosphoinositide-3 kinase and protein kinase C. *Blood* 2000; **95**: 2505–13.
9 Kawabata K, Ujikawa M, Egawa T *et al.* A cell-autonomous requirement for CXCR4 in long-term lymphoid and myeloid reconstitution. *Proc Natl Acad Sci USA* 1999; **96**: 5663–7.
10 Peled A, Petit I, Kollet O *et al.* Dependence of human stem cell engraftment and repopulation of NOD/SCID mice on CXCR4. *Science* 1999; **283**: 845–8.
11 Zeelenberg IS, Ruuls-Van Stalle L, Roos E. The chemokine receptor CXCR4 is required for outgrowth of colon carcinoma micrometastases. *Cancer Res* 2003; **63**: 3833–9.
12 Phillips RJ, Burdick MD, Lutz M, Belperio JA, Keane MP, Strieter RM. The stromal derived factor-1/CXCL12-CXC chemokine receptor 4 biological axis in non-small cell lung cancer metastases. *Am J Respir Crit Care Med* 2003; **167**: 1676–86.
13 Taichman RS, Cooper C, Keller ET, Pienta KJ, Taichman NS, McCauley LK. Use of the stromal cell-derived factor-1/CXCR4 pathway in prostate cancer metastasis to bone. *Cancer Res* 2002; **62**: 1832–7.
14 Hernandez PA, Gorlin RJ, Lukens JN *et al.* Mutations in the chemokine receptor gene CXCR4 are associated with WHIM syndrome, a combined immunodeficiency disease. *Nat Genet* 2003; **34**: 70–4.
15 Lefkowitz RJ, Shenoy SK. Transduction of receptor signals by beta-arrestins. *Science* 2005; **308**: 512–7.
16 Marchese A, Benovic JL. Agonist-promoted ubiquitination of the G protein-coupled receptor CXCR4 mediates lysosomal sorting. *J Biol Chem* 2001; **276**: 45 509–12.
17 Orsini MJ, Parent JL, Mundell SJ, Benovic JL, Marchese A. Trafficking of the HIV coreceptor CXCR4. Role of arrestins and identification of residues in the c-terminal tail that mediate receptor internalization. *J Biol Chem* 1999; **274**: 31 076–86.
18 Marchese A, Raiborg C, Santini F, Keen JH, Stenmark H, Benovic JL. The E3 ubiquitin ligase AIP4 mediates ubiquitination and sorting of the G protein-coupled receptor CXCR4. *Dev Cell* 2003; **5**: 709–22.
19 Darash-Yahana M, Pikarsky E, Abramovitch R *et al.* Role of high expression levels of CXCR4 in tumor growth, vascularization, and metastasis. *FASEB* 2004; **J 18**: 1240–2.
20 Vila-Coro AJ, Rodriguez-Frade JM, Martin De Ana A, Moreno-Ortiz MC, Martinez AC, Mellado M. The chemokine SDF-1alpha triggers CXCR4 receptor dimerization and activates the JAK/STAT pathway. *FASEB J* 1999; **13**: 1699–710.
21 Babcock GJ, Farzan M, Sodroski J. Ligand-independent dimerization of CXCR4, a principal HIV-1 coreceptor. *J Biol Chem* 2003; **278**: 3378–85.
22 Terrillon S, Bouvier M. Roles of G-protein-coupled receptor dimerization. *EMBO Rep* 2004; **5**: 30–4.
23 Hu H, Shioda T, Hori T *et al.* Dissociation of ligand-induced internalization of CXCR-4 from its co-receptor activity for HIV-1 Env-mediated membrane fusion. *Arch Virol* 1998; **143**: 851–61.
24 Yanagida M, Hayano T, Yamauchi Y *et al.* Human fibrillarin forms a sub-complex with splicing factor 2-associated p32, protein arginine methyltransferases, and tubulins alpha 3 and beta 1 that is independent of its association with preribosomal ribonucleoprotein complexes. *J Biol Chem* 2004; **279**: 1607–14.
25 Komano J, Miyauchi K, Matsuda Z, Yamamoto N. Inhibiting the Arp2/3 complex limits infection of both intracellular mature vaccinia virus and primate lentiviruses. *Mol Biol Cell* 2004; **15**: 5197–207.
26 Roland J, Murphy BJ, Ahr B *et al.* Role of the intracellular domains of CXCR4 in SDF-1-mediated signaling. *Blood* 2003; **101**: 399–406.
27 Haribabu B, Richardson RM, Fisher I *et al.* Regulation of human chemokine receptors CXCR4. Role of phosphorylation in desensitization and internalization. *J Biol Chem* 1997; **272**: 28 726–31.
28 Tarasova NI, Stauber RH, Michejda CJ. Spontaneous and ligand-induced trafficking of CXC-chemokine receptor 4. *J Biol Chem* 1998; **273**: 15 883–6.
29 Soda Y, Shimizu N, Jinno A *et al.* Establishment of a new system for determination of coreceptor usages of HIV based on the human glioma NP-2 cell line. *Biochem Biophys Res Commun* 1999; **258**: 313–21.
30 Zhang Y, Foudi A, Geay JF *et al.* Intracellular localization and constitutive endocytosis of CXCR4 in human CD34+ hematopoietic progenitor cells. *Stem Cells* 2004; **22**: 1015–29.
31 Mundy DI, Machleidt T, Ying YS, Anderson RG, Bloom GS. Dual control of caveolar membrane traffic by microtubules and the actin cytoskeleton. *J Cell Sci* 2002; **115**: 4327–39.
32 Rappoport JZ, Taha BW, Lemeer S, Benmerah A, Simon SM. The AP-2 complex is excluded from the dynamic population of plasma membrane-associated clathrin. *J Biol Chem* 2003; **278**: 47 357–60.
33 Rappoport JZ, Simon SM. Real-time analysis of clathrin-mediated endocytosis during cell migration. *J Cell Sci* 2003; **116**: 847–55.
34 Keyel PA, Watkins SC, Traub LM. Endocytic adaptor molecules reveal an endosomal population of clathrin by total internal reflection fluorescence microscopy. *J Biol Chem* 2004; **279**: 13 190–204.
35 Yarar D, Waterman-Storer CM, Schmid SL. A dynamic actin cytoskeleton functions at multiple stages of clathrin-mediated endocytosis. *Mol Biol Cell* 2005; **16**: 964–75.

doi: 10.1111/j.1349-7006.2007.00388.x

36 Pediani JD, Colston JF, Caldwell D, Milligan G, Daly CJ, McGrath JC. Beta-arrestin-dependent spontaneous alpha1a-adrenoceptor endocytosis causes intracellular transportation of alpha-blockers via recycling compartments. *Mol Pharmacol* 2005; **67**: 992–1004.
37 Segredo V, Burford NT, Lameh J, Sadee W. A constitutively internalizing and recycling mutant of the mu-opioid receptor. *J Neurochem* 1997; **68**: 2395–404.
38 Gulino AV, Moratto D, Sozzani S *et al.* Altered leukocyte response to CXCL12 in patients with warts hypogammaglobulinemia, infections, myelokathexis (WHIM) syndrome. *Blood* 2004; **104**: 444–52.
39 Kawai T, Choi U, Whiting-Theobald NL *et al.* Enhanced function with decreased internalization of carboxy-terminus truncated CXCR4 responsible for WHIM syndrome. *Exp Hematol* 2005; **33**: 460–8.
40 Balabanian K, Lagane B, Pablos JL *et al.* WHIM syndromes with different genetic anomalies are accounted for by impaired CXCR4 desensitization to CXCL12. *Blood* 2005; **105**: 2449–57.

QAD 200762

Inhibiting lentiviral replication by HEXIM1, a cellular negative regulator of the CDK9/cyclin T complex

Saki Shimizua[a,b], Emiko Urano[a], Yuko Futahashi[a], Kosuke Miyauchi[a], Maya Isogai[a], Zene Matsuda[a], Kyoko Nohtomi[a], Kazunari Onogi[a], Yutaka Takebe[a], Naoki Yamamoto[a,b] and Jun Komano[a]

Objective: Tat-dependent transcriptional elongation is crucial for the replication of HIV-1 and depends on positive transcription elongation factor b complex (P-TEFb), composed of cyclin dependent kinase 9 (CDK9) and cyclin T. Hexamethylene bisacetamide-induced protein 1 (HEXIM1) inhibits P-TEFb in cooperation with 7SK RNA, but direct evidence that this inhibition limits the replication of HIV-1 has been lacking. In the present study we examined whether the expression of FLAG-tagged HEXIM1 (HEXIM1-f) affected lentiviral replication in human T cell lines.

Methods: HEXIM1-f was introduced to five human T cell lines, relevant host for HIV-1, by murine leukemia virus vector and cells expressing HEXIM1-f were collected by fluorescence activated cell sorter. The lentiviral replication kinetics in HEXIM1-f-expressing cells was compared with that in green fluorescent protein (GFP)-expressing cells.

Results: HIV-1 and simian immunodeficiency virus replicated less efficiently in HEXIM1-f-expressing cells than in GFP-expressing cells of the five T cell lines tested. The viral revertants were not immediately selected in culture. In contrast, the replication of vaccinia virus, adenovirus, and herpes simplex virus type 1 was not limited. The quantitative PCR analyses revealed that the early phase of viral life cycle was not blocked by HEXIM1. On the other hand, *tat*-dependent transcription in HEXIM1-f-expressing cells was substantially repressed as compared with that in GFP-expressing cells.

Conclusion: These data indicate that HEXIM1 is a host factor that negatively regulates lentiviral replication specifically. Elucidating the regulatory mechanism of HEXIM1 might lead to ways to control lentiviral replication.

AIDS 2007, **21**:1–8

Keywords: CDK9, cyclin T, HEXIM1, lentivirus, *tat*

Introduction

Activation of transcription elongation requires the positive transcription elongation factor b complex (P-TEFb) composed of cyclin dependent kinase 9 (CDK9) and cyclin T1, T2, or K [1]. P-TEFb is essential for efficient transcriptional elongation from the promoter of human immunodeficiency virus type 1 (HIV-1), the long terminal repeat (LTR) (reviewed in [2,3]). The functional interaction between P-TEFb and the viral protein Tat has been well studied. Immediately after viral transcription starts at the LTR of the integrated proviral genome, the nascent viral transcript forms a three-dimensional structure called TAR. In the presence of P-TEFb, Tat binds to TAR. Through the Tat–TAR interaction, Tat activates P-TEFb and therefore assures the efficient

From the [a]AIDS Research Center, National Institute of Infectious Diseases, Tokyo, and the [b]Department of Molecular Virology, Tokyo Medical and Dental University, Tokyo, Japan.

Correspondence to Jun Komano, AIDS Research Center, National Institute of Infectious Diseases, 1-23-1 Toyama, Shinjuku, Tokyo 162-8640, Japan.

E-mail: ajkomano@nih.go.jp

AQ1 Received: ?? ??; revised: ?? ??; accepted: ?? ??.

ISSN 0269-9370 © 2007 Lippincott Williams & Wilkins

completion of viral gene transcription and the propagation of HIV-1.

Recently, the regulatory mechanisms of P-TEFb function have been elucidated. In 2001, the interaction of P-TEFb with 7SK RNA was found to be necessary to inactivate the kinase activity of CDK9 within P-TEFb [4–6]. However, the binding of 7SK RNA alone is not sufficient to inactivate P-TEFb. More recently, Yik *et al.* demonstrated that the inactivation of P-TEFb requires hexamethylene bisacetamide-induced protein 1 (HEXIM1; synonyms CLP1, MAQ1, and HIS1) [7–9]. The inactivation of P-TEFb by the HEXIM1-7SK RNA complex appears to regulate the transcriptional elongation of cellular genes.

The HEXIM1-7SK RNA complex has been shown to physically compete with Tat for binding to P-TEFb [10]. In agreement with this finding, HEXIM1 was shown to inhibit Tat-dependent transcription from the HIV-1 LTR in transient transfection assays [8,11,12]. However, no data demonstrating that HEXIM1 is able to limit HIV-1 replication has been provided. Here we provide direct experimental evidence that the constitutive expression of HEXIM1 specifically limits lentiviral replication.

Methods

Plasmids

The FLAG-tagged HEXIM1 expression constructs were generated by reverse-transcription PCR using RNA isolated from CEM cells as templates. The primers used were 5′-CACCTCGAGCCACCATGGACTACAAAGACGATGACGACAAGGCCGAGCCATTCTTGTC-3′ and 5′-CAATTGCTAGTCTCCAAACTTGGAAAGCGGCGC-3′′ for amino terminus FLAG tagging, and 5′-CACCTCGAGCCACCATGGCCGAGCCATTCTTGTCAGAATATC-3′ and 5′-CAATTGCTAGTCGTCATCGTCTTTGTAGTCGTCTCCAAACTTGGAAAGCGGCGCTC-3′ for carboxy terminus FLAG tagging. The *Xho*I-*Mfe*I fragments of the PCR products were cloned into the *Xho*I-*Mfe*I sites of pCMMP IRES GFP, generating pCMMP f-HEXIM1 and pCMMP HEXIM1-f [13]. The cytomegalovirus (CMV) promoter-driven *gag-pol* expression vector psyn*gag-pol* has been previously described by Wagner *et al.* [14] and pLTR*gag-pol* was constructed by cloning the *Mlu*I-*Hin*dIII fragment encoding the LTR from pNL-luc [15] into the *Mlu*I-*Hin*dIII sites of psyn*gag-pol*. The tax expressing plasmid pCGtax and pHTLV LTR luciferase were kindly provided by Dr. Watanabe (Tokyo Medical Institute). The *tat*-expressing plasmid pSVtat was a generous gift from Dr. Freed (National Cancer Institute-Frederick, Frederick, Maryland,USA). The plasmid pLTR-luc has been described previously (Miyauchi *et al.*, *Antiviral Chemistry and Chemotherapy*, in press). The following plasmids have been described previously by Komano *et al.* [13]: pVSV-G, pMD*gag-pol*, pTM3Luci, phRL-CMV and pSIVmac239ΔnefLuc.

Cells and transfection

All the mammalian cells were maintained in RPMI 1640 (Sigma, St Louis, Missouri, USA) supplemented with 10% fetal bovine serum (Japan Bioserum, Tokyo, Japan), penicillin and streptomycin (Invitrogen, Tokyo, Japan). Cells were incubated at 37°C in a humidified 5% CO_2 atmosphere. Cells were transfected using Lipofectamine 2000 according to the manufacturer's protocol (Invitrogen).

Western blotting

Cells were lysed with sample buffer, sonicated, and boiled for 5 min. Samples were separated on 8% sodium dodecyl sulfate-polyacrylamide gel electrophoresis gels and transferred to polyvinylidene difluoride membranes (Millipore, Billerica, Massachusetts, USA) for western blotting according to standard techniques. Membranes were blocked with Tris-buffered saline containing 0.05% Tween-20 (TBS-T) containing 5% (w/v) non-fat skim milk (Yuki-Jirushi, Tokyo, Japan) for 1 h at room temperature and incubated with primary antibodies including the M2 anti-FLAG epitope monoclonal antibody (Sigma), an anti-actin monoclonal antibody (MAB1501R; Chemicon/Millipore, Billerica, Massachusetts, USA), an anti-cyclin T1 rabbit polyclonal antibody (H-245; Santa Cruz Biotechnology, Santa Cruz, California, USA), an anti-cyclin T2a/b goat polyclonal antibody (A-20; Santa Cruz), an anti-p24 monoclonal antibody (183-H12-5C; NIH AIDS Research and Reference Reagent Program), an anti-HIS1 chicken polyclonal antibody (N-150; GenWay), and an anti-Bip/GRP78 monoclonal antibody (clone 40; BD Biosciences/Transduction Laboratories, San Jose, California, USA) for 1 h at room temperature. Membranes were washed with TBS-T and incubated with appropriate second antibodies including biotinylated anti-goat (GE Healthcare Bio-Sciences, Piscataway, New Jersey, USA) or anti-chicken IgY (Promega, Madison, Wisconsin, USA), and EnVision+ (Dako, Glostrup, Denmark) for 1 h at room temperature. For a tertiary probe, we used horseradish peroxidase (HRP)-streptavidine (GE Healthcare) if necessary. Signals were visualized with an LAS3000 imager (Fujifilm, Tokyo, Japan) after treating the membranes with the Lumi-Light Western Blotting Substrate (Roche Diagnostics GmbH, Mannheim, Germany).

Reporter assay

Luciferase activity was measured 48 h after transfection or infection using a DualGlo assay kit (Promega) according to the manufacturer's protocol. The beta-galactosidase activity was measured using a LumiGal assay kit (BD Biosciences/Clontech, San Jose, California, USA) according to the manufacturer's protocol. The chemilu-

minescence was detected with a Veritas luminometer (Promega).

Monitoring viral replication

To monitor HIV-1 replication, the culture supernantants were subjected to either a reverse transcriptase assay [16] or an enzyme-linked immunosorbent assay (ELISA) to detect p24 antigens using a Retro TEK p24 antigen ELISA kit according to the manufacturer's protocol (Zepto Metrix, Buffalo, New York, USA). For simian immunodeficiency virus (SIV) a p27 antigen ELISA kit was used according to the manufacturer's protocol (Zepto Metrix). The signals were measured with a Multiskan Ex microplate photometer (ThermoLabsystems, Helsinki, Finland). For vaccinia virus, adenovirus, and herpes simplex virus (HSV)-1, the activity of reporter genes was measured as previously described [13].

Generating viruses

To produce HIV-1 and SIV, 293T cells were transfected with plasmids encoding proviral DNA of HIV-1 (pHXB2) or pSIVmac239ΔnefLuc and culture supernatants containing viruses were collected at 48 h post-transfection. Murine leukemia virus (MLV) and lentiviral vectors pseudotyped with VSV-G were produced as described previously by cotransfecting 293T cells with either the pNL-Luc and pVSV-G vectors or the pMD*gag-pol*, pVSV-G, and pCMMP vectors [13]. Green fluorescent cells were sorted by fluorescence activated cell sorter (FACS) Aria (Becton Dickinson, San Jose, California, USA).

Reverse transcriptase-polymerase chain reaction

Total RNA was isolated with an RNeasy kit (Qiagen GmbH, Hilden, Germany) according to the manufacturer's instruction. The reverse transcriptase (RT)-polymerase chain reaction (PCR) assay was performed with a One Step RNA PCR Kit (Takara, Otsu, Japan), imaged by a Typhoon scanner 9400 (GE Healthcare), and quantified with Image Quant software (GE Healthcare). For the amplification of endogenous HEXIM1, the forward primer 5′-ACCACACGGAGAGCCTGCA-GAAC-3′ and the reverse primer 5′-TAGCTAAA-TTTACGAAACCAAAGCC-3′ were used. For the amplification of HEXIM1-f, the forward primer 5′-GTACCTGGAACTGGAGAAGTGCCC-3′ and the reverse primer 5′-CAATTGCTAGTCGTCATCGTC-TTTGTAGTC-3′ were used. For cyclophilin A, the forward primer 5′-CACCGCCACCATGGTCAAC-CCCACCGTGTTCTTCGAC-3′ and the reverse primer 5′-CCCGGGCCTCGAGCTTTCGAGTTGT-CCACAGTCAGCAATGG-3′ were used.

Quantitative real time polymerase chain reaction

The real time PCR reaction was performed in a DNA Engine Opticon 2 Continuous Fluorescence Detection System (Bio-Rad, Hercules, California, USA). The cellular genomic DNA and total RNA were extracted 48 h post-infection with a DNeasy kit (Qiagen) and RNeasy kit (Qiagen), respectively, according to the manufacturer's instruction. For the reagents, we used QuantiTect SYBR Green PCR and RT-PCR Kits (Qiagen). To estimate the amount of integrated HIV-1 DNA, Alu-LTR PCR was performed according to the method described previously using the following primers: for the first PCR, 5′-AACTAGGGAACCCACTGCT-TAAG-3′ and 5′-TGCTGGGATTACAGGCGTGAG-3′, and for the second PCR, 5′-AACTAGGGAACC-CACTGCTTAAG-3′ and 5′-CTGCTAGAGATTT-TCCACACTGAC-3′ [17]. The beta-globin primers have been described previously [18]. To estimate the amount of HIV-1 RNA, the second PCR primers for the Alu-LTR PCR were used. The primers for cyclophilin A are described above.

Results and discussion

The HEXIM1 cDNA tagged with a FLAG epitope at either the amino terminus (f-HEXIM1) or the carboxy terminus (HEXIM1-f) was cloned in a mammalian expression plasmid (Fig. 1a). A luciferase assay revealed that the Tat-dependent enhancement of transcription from the HIV-1 LTR was reduced by co-transfecting HEXIM1-expressing plasmids, whereas neither Tat-independent basal transcription from the HIV-1 LTR nor CMV promoter-driven transcription was affected (Fig. 1b). An oncogenic retrovirus human T cell leukemia virus type 1 (HTLV-1) encodes for *tax*, a functional homologue of HIV-1's *tat*, that utilizes P-TEFb to enhance transcription from the LTR promoter [19]. However, *tax*-dependent enhancement of transcription was not affected by HEXIM1 in similar experimental conditions (Fig. 1c). To monitor the effect of HEXIM1 on HIV-1 replication, we introduced HEXIM1-expressing plasmids into HeLa-CD4 cells along with pNL4-3, which produces replication-competent HIV-1, and measured the RT activity in the culture supernatant 1 week post-transfection. Transfecting HEXIM1-expressing plasmids decreased the RT activity in a dose-dependent manner (Fig. 1d). Next, we asked whether the inhibition of viral replication was specific to HIV-1 by examining vaccinia virus, adenovirus, and HSV-1 replication. We found that the propagation of these three viruses was not inhibited by HEXIM1-f expression (Fig. 1e–g), suggesting that the inhibition of viral replication by HEXIM1 was HIV-1-specific.

To examine whether HEXIM1 negatively affects lentiviral replication in the physiologically relevant host, we isolated human T cell lines constitutively expressing HEXIM1-f. We cloned HEXIM1-f cDNA into a pCMMP (MLV retroviral vector plasmid (Fig. 2a). The plasmid encoded an internal ribosomal entry site (IRES)-mediated green fluorescent protein (GFP)

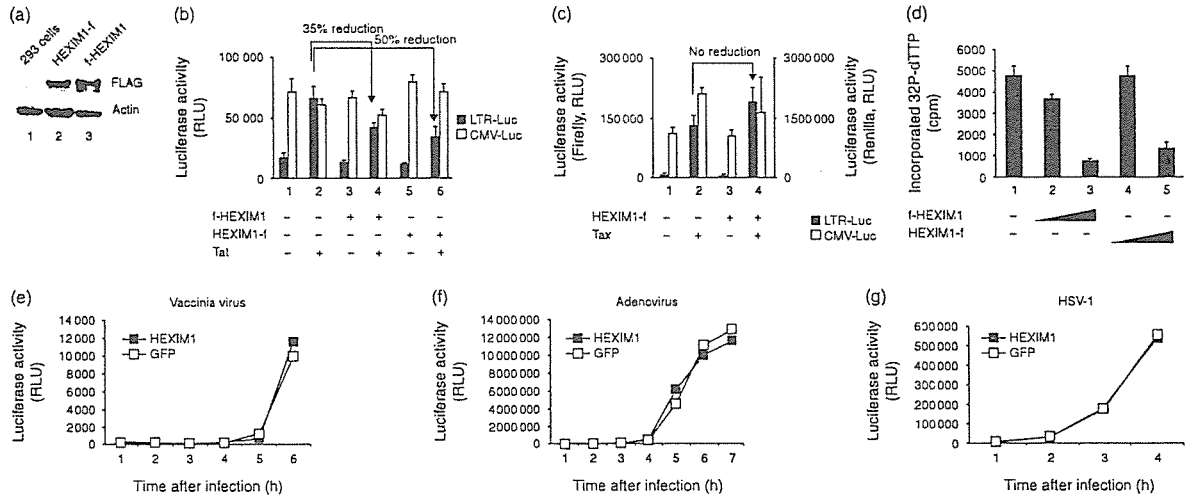

Fig. 1. Expression of hexamethylene bisacetamide-induced protein 1 (HEXIM1) specifically inhibits HIV-1 replication. (a) Detection of HEXIM1 cDNA tagged with a FLAG epitope at either the amino terminus (f-HEXIM1) or the carboxy terminus (HEXIM1-f) by western blot analysis in transiently transfected 293 cells (upper panel, approximately 65 kD). A western blot against actin is shown as a loading control (lower panel). (b) Expressing FLAG-tagged HEXIM1 decreased the luciferase activity driven by HIV-1 long terminal repeat (LTR) promoter in the presence of Tat (lanes 4 and 6, LTR-Luc, solid bars). However, FLAG-tagged HEXIM1 did not affect the expression of renilla luciferase from co-transfected plasmid driven by the cytomegalovirus (CMV) promoter (CMV-Luc, open bars). Representative data from three independent experiments done in triplicate are shown. Cells were transfected with 0.8 μg HEXIM1-expressing plasmid for the indicated lanes, 0.1 μg of pSV*tat* for the indicated lanes, and 0.1 μg of pLTR-Luc and 0.5 μg for phRL/CMV for all lanes. (c) Expressing FLAG-tagged HEXIM1 did not decrease the luciferase activity driven by HTLV-1 LTR promoter in the presence of Tax (lanes 2 and 4, LTR-Luc, solid bars) as well as renilla luciferase driven by the CMV promoter (CMV-Luc, open bars). Representative data from three independent experiments done in triplicate are shown. Cells were transfected with 0.8 μg of HEXIM1-expressing plasmid for the indicated lanes, 0.1 μg of pCGtax for the indicated lanes, and 0.1 μg of pHTLV LTR Luc and 0.5 μg for phRL/CMV for all lanes. (d) The dose-dependent reduction of HIV-1 production by transfection of HEXIM1-encoding plasmids (0.1 μg for lanes 2 and 4, 0.4 μg for lanes 3 and 5) along with a plasmid producing infectious HIV-1 (pNL4-3, 0.1 μg) in HeLa-CD4 cells. (e–g) Expressing HEXIM1-f did not limit the replication of vaccinia virus (e), adenovirus (f), or HSV-1 (g) in 293T cells. The *y*-axis represents the reporter gene activity, which reflects viral replication. Representative data from three independent experiments are shown. GFP, green fluorescent protein; RLU, relative light unit.

expression cassette, so that MLV vector-infected cells could be readily identified by the green fluorescence. Human T cell lines, including SUP-T1, MOLT-4, CEM, Jurkat, and M8166 were infected with MLV pseudotyped with vesicular stomatitis virus glycoprotein (VSV-G), and GFP-positive cells were collected with a FACS (Fig. 2a). For the negative control, we used MLV expressing GFP only. The successful introduction of HEXIM1-f into the cells was verified by RT-PCR and Western blot analysis (Fig. 2b and c). The total HEXIM1 protein expression in HEXIM1-f-transduced cells was approximately 3.7-, 1.5-, 2.0-, 4.8-, and 1.8-fold higher than in GFP-transduced cells in the CEM, Jurkat, MOLT-4, SUP-T1, and M8166 cell lines, respectively (Fig. 2c). To our surprise, the HEXIM1-f-expressing T cell lines remained GFP-positive, and therefore HEXIM1-f-positive, for more than 6 months and proliferated at rates almost indistinguishable from GFP-expressing cells. The expression levels of cyclin T1, cyclin T2, actin, and Bip/GRK78 in HEXIM1-f-expressing cells were almost identical to those in GFP-expressing cells, suggesting that the gene expression did not compensate the upregulated HEXIM1 (Fig. 2b and c). Expression of cyclin T2 was undetectable in M8166 cells (Fig. 2c). Similarly, HEXIM1-f expression did not affect the cell surface levels of the HIV-1 receptors CD4 and CXCR4 as demonstrated by FACS analysis (data not shown). These data indicate that the expression of HEXIM1-f did not reach levels where the physiological regulation of P-TEFb blocked cellular gene transcription.

The replication kinetics of HIV-1 or SIV was monitored by measuring the accumulation of viral capsid antigen in the culture medium. Strikingly, HIV-1 replicated more slowly in cells of all four T cell lines expressing HEXIM1-f than in cells expressing GFP (Fig. 2d–g). Similarly, HEXIM1-f-expressing M8166 cells supported SIV replication less efficiently than did GFP-expressing M8166 cells (Fig. 2h). Interestingly, the magnitude of HIV-1 replication delay was the most substantial in SUP-T1 cells, in which the levels of endogenous HEXIM1 were the lowest among the four cell lines tested for HIV-1 replication (Fig. 2c). Similar observations were made when the HIV-1 infection experiments were repeated,

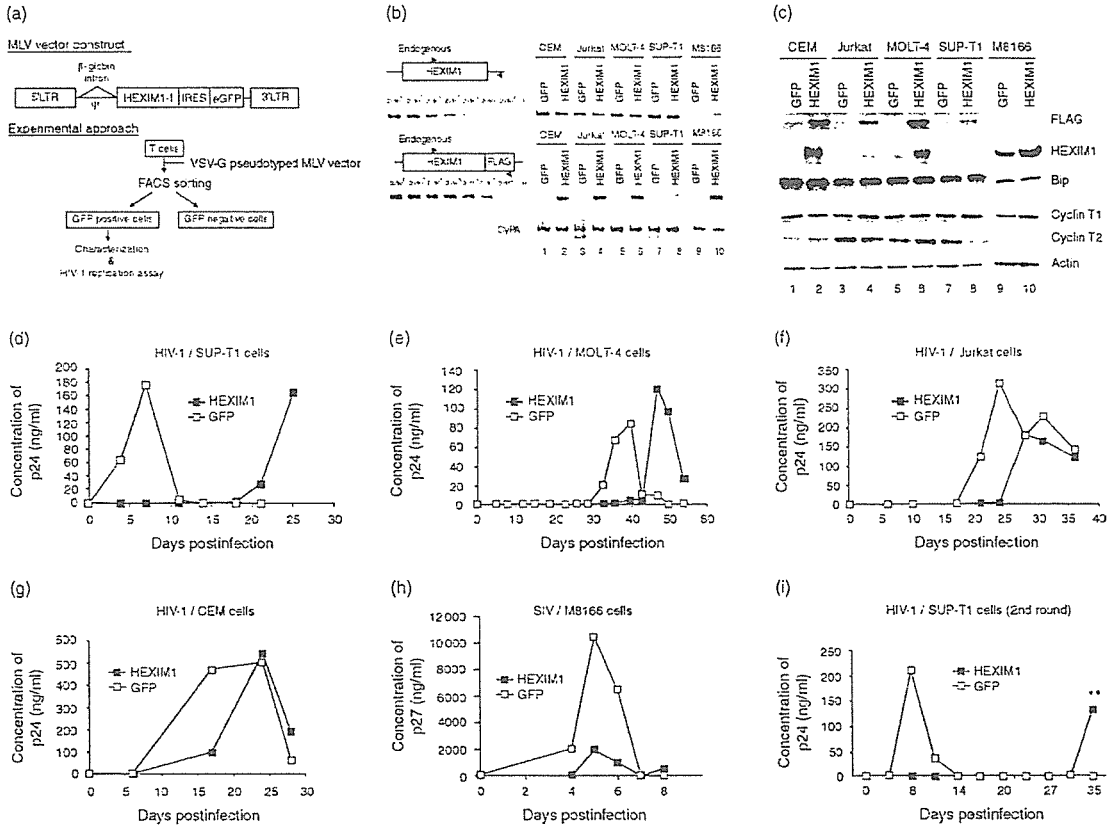

Fig. 2. Lentiviral replication is inhibited in various T cell lines constitutively expressing hexamethylene bisacetamide-induced protein 1 (HEXIM-1) cDNA tagged with a FLAG epitope at the carboxy terminus (HEXIM1-f). (a) The genomic organization of the retroviral vector expressing HEXIM1-f and a schematic representation of the experimental approach. (b) Detection of endogenous HEXIM1 and murine leukemia virus (MLV)-transduced HEXIM1-f (exogenous) mRNA by reverse transcriptase-polymerase chain reaction in green fluorescent protein (GFP)- and HEXIM1-f-expressing cells. The primer design is drawn schematically. Amplification efficiency was examined by using a known number of templates as standards for HEXIM1. Cyclophilin A (CyPA) was amplified to ensure the quality of the RNA. (c) Western blot analysis demonstrating expression of HEXIM1-f (denoted FLAG), endogenous HEXIM1 (HEXIM1), Bip, cyclin T1, cyclin T2, and actin in isolated T cell lines. (d–g) Replication profiles of HIV-1 (HXB2) in SUP-T1 (d), MOLT-4 (e), Jurkat (f), and CEM (g) cells either expressing HEXIM1-f or GFP alone. Representative data from two or three independent experiments are shown. (h) Replication profile of SIV in M8166 cells either expressing HEXIM1-f or GFP alone. Representative data from two independent experiments are shown. (i) The replication profiles of HIV-1 recovered from SUP-T1/HEXIM1-f cells (asterisk in Fig. 2d) in fresh SUP-T1/GFP or SUP-T1/HEXIM1-f. LTR, long terminal repeat.

indicating that the expression of functional HEXIM1-f did not change over the course of the replication monitoring. We tested whether the viruses emerged in HEXIM1-f-expressing cells were 'revertants' that might be able to replicate in HEXIM1-f-expressing cells as fast as in GFP-expressing cells. To address this, we recovered virus-containing culture supernatants from SUP-T1/HEXIM1-f cells at the peak of replication kinetics (asterisk, Fig. 2d). Then, both fresh SUP-T1/GFP and SUP-T1/HEXIM1-f were infected with the recovered virus and the replication kinetics was monitored. However, HIV-1 still replicated in SUP-T1/HEXIM1-f cells more slowly than in SUP-T1/GFP cells (Fig. 2i), akin to the original profiles (Fig. 2d), and the nucleotide sequences of LTR and *tat*, the primary targets of HEXIM1, remained unchanged (double asterisk in Fig. 2i). In addition, no mutations were found in viruses propagated in GFP-expressing SUP-T1 cells. Similar observations were made in MOLT-4 cells (data not shown). These data provide direct evidence that the expression of HEXIM1 inhibits lentiviral replication in human T cell lines.

Based on our experimental observations as well as the reported functions of HEXIM1, we assumed that the ability of HEXIM1 to limit HIV-1 replication was mostly due to the inhibition of Tat/P-TEFb-dependent transcriptional elongation. However, it was possible that HEXIM1 might also have targeted other viral replication steps. To test this possibility, we examined the viral entry and production processes separately. The efficiency of viral entry was analyzed by measuring the efficiency of

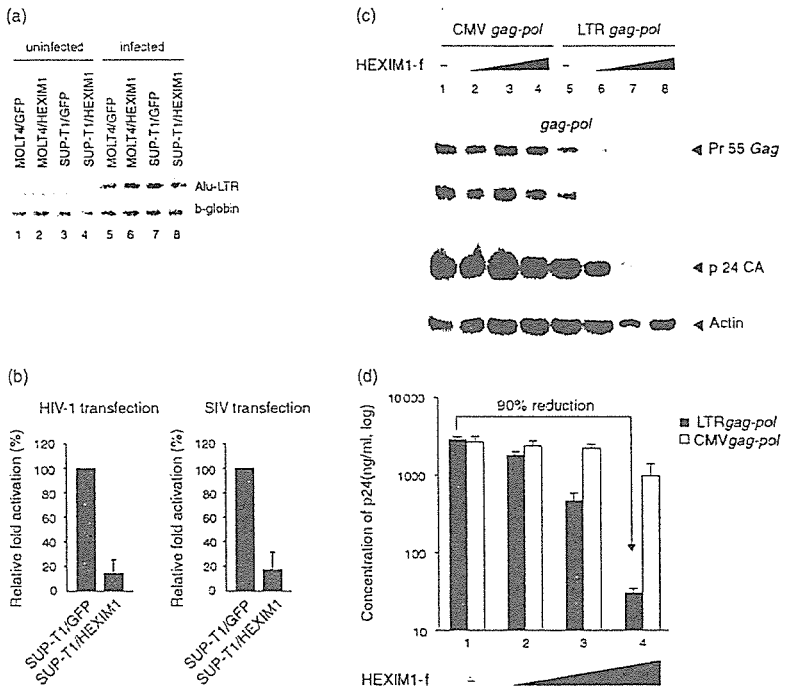

Fig. 3. Hexamethylene bisacetamide-induced protein 1 (HEXIM1) cDNA tagged with a FLAG epitope at the carboxy terminus (HEXIM1-f) does not affect the efficiency of viral integration or post-translational processes. (a) The Alu-long terminal repeat (LTR) and beta-globin polymerase chain reaction products from VSV-G-pseudotyped HIV-1-infected MOLT-4 and SUP-T1 cells expressing either green fluorescent protein (GFP) or HEXIM1-f alone were separated in an agarose gel and photographed. (b) The luciferase activities in SUP-T1/GFP or SUP-T1/HEXIM1-f cells electroporated with 10 μg of a plasmid encoding LTR-driven firefly luciferase plus 1 μg of phRL/cytomegalovirus (CMV). The firefly luciferase activity normalized to renilla luciferase activity in SUP-T1/GFP cells was set to 100%. The error bars represent the standard deviation of three independent experiments. (c) Western blot analysis showing Gag and its cleaved products expressed from either CMV promoter- or LTR promoter-driven *gag-pol* expression plasmid in the presence of pSVtat (0.1 μg, all lanes) and increasing amounts of HEXIM1-f (0.2 μg for lanes 2 and 6, 0.6 μg for lanes 3 and 7, and 2.0 μg for lanes 4 and 8). (d) The amount of p24 produced in the culture supernatant from cells analyzed in Fig. 3c was measured by enzyme-linked immunosorbent assay. Representative data from three independent experiments done in triplicate are shown. SIV, simian immunodeficiency virus.

viral integration. SUP-T1/GFP or SUP-T1/HEXIM1-f cells were infected with a replication-incompetent HIV-1 vector pseudotyped with VSV-G that expresses luciferase upon successful infection. We conducted an Alu-LTR PCR assay to detect the integrated viral genome. PCR products were detected only from HIV-1-infected cells (Fig. 3a). The signal intensities of Alu-LTR PCR products from GFP- and HEXIM1-f-experssing cells were similar. To compare the efficiency of viral infection as well as transcription quantitatively, we employed a real time PCR technique. Some infected cells were collected for an Alu-LTR PCR assay to quantify the amount of integrated viral genome, and the rest were processed to measure the amount of viral transcript as well as the luciferase activity. The amount of Alu-LTR PCR product from SUP-T1/HEXIM1-f cells was 3.5- and 3.3-fold more to that from SUP-T1/GFP cells from two independent experiments, respectively (Table 1). These data suggest that the efficiency of viral integration was not inhibited in HEXIM1-f-expressing SUP-T1 cells. In contrast, the relative abundance of HIV-1 transcript expressed in SUP-T1/HEXIM1-f cells was substantially decreased to 0.03 and 2.9% relative to SUPT1/GFP cells (Table 1). Furthermore, the luciferase activities were 200-fold lower in SUP-T1/HEXIM1-f cells than in SUP-T1/GFP cells (Table 1). Similar data was obtained from MOLT-4 cells infected with HIV-1 pseudotyped with VSV-G (data not shown). The transfection of plasmids encoding reporter viral DNA can bypass the viral entry and make it possible to measure the effect of HEXIM1 on LTR-driven transcription and translation. Consistent with above data, transfecting pNL-Luc into SUP-T1/HEXIM1-f cells gave significantly lower luciferase activities than SUP-T1/GFP cells (Fig. 3b, left). Similar data were obtained using pSIVmac239ΔnefLuc (Fig. 3b, right). These data strengthen the possibility that HEXIM1 targets post-integration processes.

To test this further, we analyzed the efficiency of post-transcriptional processes with a transient transfection assay measuring the amount of Pr55 Gag, a viral gene product, and virus-like particles (VLPs) produced in the culture

Table 1. Effect of hexamethylene bisacetamide-induced protein 1 (HEXIM1) cDNA tagged with a FLAG epitope at the carboxy terminus (HEXIM1-f) on viral entry and transcription in SUP-T1 cells examined by quantitative real time polymerase chain reaction.

		Integrated HIV-1 genome			HIV-1 transcript			Luciferase activity	
Exp.	Transduced gene	Alu-LTR (copy)	β-globin (copy)	Normalized[a] (%)	HIV-1 RNA (copy)	CyPA (copy)	Normalized[b] (%)	RLU[c]	Normalized[d] (%)
1	GFP	5.2×10^5	6.7×10^6	100.0	1.6×10^6	6.8×10^7	100.0	3.2×10^5	100.0
	HEXIM1-f	2.0×10^6	7.4×10^6	351.3	6.7×10^1	1.0×10^8	0.03	1.5×10^3	0.5
2	GFP	4.6×10^6	1.8×10^7	100.0	3.1×10^8	8.9×10^7	100.0	7.1×10^5	100.0
	HEXIM1-f	1.6×10^7	1.9×10^7	333.2	9.4×10^6	9.3×10^7	2.9	3.4×10^3	0.5

[a]The number of Alu-long terminal repeat (LTR) products divided by the number of beta-globin products in SUP-T1/GFP is set to 100%. The abundance of Alu-LTR products in SUP-T1/HEXIM1-f relative to SUP-T1/green fluorescent protein (GFP) is shown.
[b]The number of HIV-1 RNA transcripts in SUP-T1/GFP divided by the number of cyclophilin A (CyPA) transcripts is set to 100%. The abundance of HIV-1 RNA in SUP-T1/HEXIM1-f relative to SUP-T1/GFP is shown.
[c]The luciferase activity is shown by relative light unit (RLU).
[d]The luciferase activity in SUP-T1/GFP is set to 100%. The luciferase activity in SUP-T1/HEXIM1-f relative to SUP-T1/GFP is shown.

supernatants. For this purpose, we used the CMV promoter-driven *gag-pol* expression plasmid, because HEXIM1-f did not affect CMV-driven transcription (Fig. 1b). At the levels of HEXIM1-f where LTR-driven Tat-dependent transcription was drastically inhibited (Fig. 3c, lanes 7, 8), the amount of CMV promoter-driven Gag expression was almost identical to that in the absence of HEXIM1-f (Fig. 3c, lanes 1–4). Furthermore, the processing pattern of Pr55 Gag in the presence of HEXIM1-f was identical to that in its absence (Fig. 3c). These data indicate that HEXIM1-f did not inhibit the transcription from a Tat-independent promoter, the translation of viral protein, or the protease activity of HIV-1. Finally, the potential effect of HEXIM1 on viral budding was examined. To do this, the amount of p24 CA in the culture supernatant of transfected cells was quantified as a representation of the amount of VLP. Expressing HEXIM1-f reduced VLP production from cells co-transfected with pLTR*gag-pol* and pSVtat at levels comparable to the protein expression levels (Fig. 3c and d). In contrast, expressing HEXIM1-f did not reduce the amount of VLP produced by cells co-transfected with pCMV*gag-pol* and pSVtat in conditions in which Tat-dependent LTR transcription was substantially inhibited (Fig. 3c and d). Taken together, this indicates that HEXIM1-f lowers the efficiency of Tat-dependent transcription from LTR promoter but does not block the efficiency of the late phase of the viral life cycle including translation, Gag's assembly, and budding. Thus, it is likely that HEXIM1 primarily targets Tat/P-TEFb-dependent transcription to inhibit HIV-1 replication.

Our findings demonstrated that HEXIM1, a cellular P-TEFb inhibitor, is a specific negative regulator of lentiviral replication in human T cell lines. The replication of vaccinia virus, adenovirus, and HSV-1 were not affected by HEXIM1-f expression; however, the *tat*-dependent transcription of the LTR promoter of both HIV-1 and SIV was reduced by HEXIM1-f. HEXIM1 limited replication of HIV-1 dramatically at levels where it did not visibly affect cell physiology (as little as a 5-fold increase over the endogenous levels), nor were revertants immediately selected in HEXIM1-f-expressing cells. These data support the feasibility of developing HIV-1 inhibitors targeting the processes in which HEXIM1 is involved. For example, it is conceivable to hunt for a non-toxic chemical inducer for HEXIM1 since expression of HEXIM1 is induced by hexamethylene bisacetamide (HMBA) that is considerably toxic for cells [20].

P-TEFb has been shown to support transcription of the *c-myc* and CIITA transcription factors (reviewed in [21,22]). The functions of these transactivators are critical for cell proliferation, but in this study constitutive expression of HEXIM1-f, which reduces P-TEF-b activity, did not affect the cell proliferation of human T cell lines, the human epithelial cell lines HEK293 or the NP2 glioblastoma cell lines (data not shown). How can this be explained? Very recently, a high-molecular-weight bromodomain protein, Brd4, was found to function as a 'cellular *tat*' [23,24]. Interestingly, it was shown that Brd4 binds not only to cyclin T1 but also to cyclin T2, a widely expressed variant of cyclin T, to which HEXIM1 binds but Tat does not [23–25]. We hypothesize that Brd4 might be able to recruit and activate P-TEFb more efficiently than does Tat, leaving cellular transcription unaffected by the upregulated expression of HEXIM1 from the retroviral vector. An alternative possibility comes from the fact that HEXIM1 does not interact with the ubiquitously expressed cyclin K, which functions as a P-TEFb component. It is possible that Tat is not able to utilize P-TEFb consisting of CDK9 and cyclin K but Brd4 can, such that cyclin K may substitute for cyclin T1 to support Brd4-mediated cellular gene transcription.

Acknowledgements

We thank Dr. Tsutomu Murakami for the critical reading of the manuscript. This work was partly supported by Japan Health Science Foundation, Japanese Ministry of

Health, Labor and Welfare, and Japanese Ministry of Education, Culture, Sports, Science and Technology.

Sponsorship: This work was partly supported by Japan Health Science Foundation, Japanese Ministry of Health, Labor and Welfare, and Japanese Ministry of Education, Culture, Sports, Science and Technology.

References

1. Marshall N, Price D. **Control of formation of two distinct classes of RNA polymerase II elongation complexes.** *Mol Cell Biol* 1992; **12**:2078–2090.
2. Kuiken C, Foley B, Hahn B, Korber B, Marx P, McCutchan F, *et al.*, editors. *HIV Sequence Compendium 2000.* Los Alamos: Theoretical Biology and Biophysics Group, Los Alamos National Laboratory, 2000.
3. Barboric M, Peterlin BM. **A new paradigm in eukaryotic biology: HIV Tat and the control of transcriptional elongation.** *PLoS Biol* 2005; **3**:e76.
4. Nguyen V, Kiss T, Michels A, Bensaude O. **7SK small nuclear RNA binds to and inhibits the activity of CDK9/cyclin T complexes.** *Nature* 2001; **414**:322–325.
5. Yang Z, Zhu Q, Luo K, Zhou Q. **The 7SK small nuclear RNA inhibits the CDK9/cyclin T1 kinase to control transcription.** *Nature* 2001; **414**:317–322.
6. Li Q, Price J, Byers S, Cheng D, Peng J, Price D. **Analysis of the large inactive P-TEFb complex indicates that it contains one 7SK molecule, a dimer of HEXIM1 or HEXIM2, and two P-TEFb molecules containing Cdk9 phosphorylated at threonine 186.** *J Biol Chem* 2005; **280**:28819–28826.
7. Michels A, Nguyen V, Fraldi A, Labas V, Edwards M, Bonnet F, *et al.* **MAQ1 and 7SK RNA interact with CDK9/cyclin T complexes in a transcription-dependent manner.** *Mol Cell Biol* 2003; **23**:4859–4869.
8. Yik J, Chen R, Pezda A, Samford C, Zhou Q. **A human immunodeficiency virus type 1 Tat-like arginine-rich RNA-binding domain is essential for HEXIM1 to inhibit RNA polymerase II transcription through 7SK snRNA-mediated inactivation of P-TEFb.** *Mol Cell Biol* 2004; **24**:5094–5105.
9. Barboric M, Kohoutek J, Price J, Blazek D, Price D, Peterlin B. **Interplay between 7SK snRNA and oppositely charged regions in HEXIM1 direct the inhibition of P-TEFb.** *EMBO J* 2005; **24**:4291–4303.
10. Schulte A, Czudnochowski N, Barboric M, Schonichen A, Blazek D, Peterlin B, Geyer M. **Identification of a cyclin T-binding domain in Hexim1 and biochemical analysis of its binding competition with HIV-1 Tat.** *J Biol Chem* 2005; **280**:24968–24977.
11. Fraldi A, Varrone F, Napolitano G, Michels A, Majello B, Bensaude O, Lania L. **Inhibition of Tat activity by the HEXIM1 protein.** *Retrovirology* 2005; **2**:42.
12. Michels A, Fraldi A, Li Q, Adamson T, Bonnet F, Nguyen V, *et al.* **Binding of the 7SK snRNA turns the HEXIM1 protein into a P-TEFb (CDK9/cyclin T) inhibitor.** *EMBO J* 2004; **23**:2608–2619.
13. Komano J, Miyauchi K, Matsuda Z, Yamamoto N. **Inhibiting the Arp2/3 complex limits infection of both intracellular mature vaccinia virus and primate lentiviruses.** *Mol Biol Cell* 2004; **15**:5197–5207.
14. Wagner R, Graf M, Bieler K, Wolf H, Grunwald T, Foley P, Uberla K. **Rev-independent expression of synthetic gag-pol genes of human immunodeficiency virus type 1 and simian immunodeficiency virus: implications for the safety of lentiviral vectors.** *Hum Gene Ther* 2000; **11**:2403–2413.
15. Masuda T, Planelles V, Krogstad P, Chen I. **Genetic analysis of human immunodeficiency virus type 1 integrase and the U3 att site: unusual phenotype of mutants in the zinc finger-like domain.** *J Virol* 1995; **69**:6687–6696.
16. Willey R, Smith D, Lasky L, Theodore T, Earl P, Moss B, *et al.* **In vitro mutagenesis identifies a region within the envelope gene of the human immunodeficiency virus that is critical for infectivity.** *J Virol* 1988; **62**:139–147.
17. Butler SL, Hansen MS, Bushman FD. **A quantitative assay for HIV DNA integration in vivo.** *Nat Med* 2001; **7**:631–634.
18. Graf Einsiedel H, Taube T, Hartmann R, Wellmann S, Seifert G, Henze G, Seeger K. **Deletion analysis of p16(INKa) and p15(INKb) in relapsed childhood acute lymphoblastic leukemia.** *Blood* 2002; **99**:4629–4631.
19. Zhou M, Lu H, Park H, Wilson-Chiru J, Linton R, Brady JN. **Tax interacts with P-TEFb in a novel manner to stimulate human T-lymphotropic virus type 1 transcription.** *J Virol* 2006; **80**:4781–4791.
20. Kusuhara M, Nagasaki K, Kimura K, Maass N, Manabe T, Ishikawa S, *et al.* **Cloning of hexamethylene-bis-acetamide-inducible transcript, HEXIM1, in human vascular smooth muscle cells.** *Biomed Res* 1999; **20**:273–279.
21. Price DH. **P-TEFb, a cyclin-dependent kinase controlling elongation by RNA polymerase II.** *Mol Cell Biol* 2000; **20**:2629–2634.
22. Garriga J, Grana X. **Cellular control of gene expression by T-type cyclin/CDK9 complexes.** *Gene* 2004; **337**:15–23.
23. Jang M, Mochizuki K, Zhou M, Jeong H, Brady J, Ozato K. **The bromodomain protein Brd4 is a positive regulatory component of P-TEFb and stimulates RNA polymerase II-dependent transcription.** *Mol Cell* 2005; **19**:523–534.
24. Yang Z, Yik J, Chen R, He N, Jang M, Ozato K, Zhou Q. **Recruitment of P-TEFb for stimulation of transcriptional elongation by the bromodomain protein Brd4.** *Mol Cell* 2005; **19**:535–545.
25. Napolitano G, Licciardo P, Gallo P, Majello B, Giordano A, Lania L. **The CDK9-associated cyclins T1 and T2 exert opposite effects on HIV-1 Tat activity.** *AIDS* 1999; **13**:1453–1459.

Rapid propagation of low-fitness drug-resistant mutants of human immunodeficiency virus type 1 by a streptococcal metabolite sparsomycin

Kosuke Miyauchi, Jun Komano*, Lay Myint, Yuko Futahashi, Emiko Urano, Zene Matsuda, Tomoko Chiba, Hideka Miura, Wataru Sugiura and Naoki Yamamoto

AIDS Research Center, National Institute of Infectious Diseases, Toyama, Shinjuku, Tokyo, Japan

*Corresponding author: Tel: +81 3 5285 1111; Fax: +81 3 5285 5037; E-mail: ajkomano@nih.go.jp

Here we report that sparsomycin, a streptococcal metabolite, enhances the replication of HIV-1 in multiple human T cell lines at a concentration of 400 nM. In addition to wild-type HIV-1, sparsomycin also accelerated the replication of low-fitness, drug-resistant mutants carrying either D30N or L90M within HIV-1 protease, which are frequently found mutations in HIV-1-infected patients on highly active antiretroviral therapy (HAART). Of particular interest was that replication enhancement appeared profound when HIV-1 such as the L90M-carrying mutant displayed relatively slower replication kinetics. The presence of sparsomycin did not immediately select the fast-replicating HIV-1 mutants in culture. In addition, sparsomycin did not alter the 50% inhibitory concentration (IC_{50}) of antiretroviral drugs directed against HIV-1 including nucleoside reverse transcriptase inhibitors (lamivudine and stavudine), non-nucleoside reverse transcriptase inhibitor (nevirapine) and protease inhibitors (nelfinavir, amprenavir and indinavir). The IC_{50}s of both zidovudine and lopinavir against multidrug resistant HIV-1 in the presence of sparsomycin were similar to those in the absence of sparsomycin. The frameshift reporter assay and Western blot analysis revealed that the replication-boosting effect was partly due to the sparsomycin's ability to increase the –1 frameshift efficiency required to produce the *Gag–Pol* transcript. In conclusion, the use of sparsomycin should be able to facilitate the drug resistance profiling of the clinical isolates and the study on the low-fitness viruses.

Keywords: drug resistant mutants, enhancement of replication, HIV-1, low-fitness mutants, sparsomycin

Introduction

Highly active antiretroviral therapy (HAART) has been successful in controlling the progression of AIDS caused by HIV-1. However, HAART has accelerated the emergence and spread of multidrug-resistant HIV-1. Once drug-resistant HIV-1 occurs in a HIV-1-infected patient, the success rate of HAART drops substantially. Resistance testing has been shown to be valuable to optimize HAART against HIV-1 infection (Hirsch *et al.*, 2000; Rodriguez-Rosado *et al.*, 1999). Profiling drug resistance might be necessary even before the initiation of HAART because of the spread of drug-resistant HIV-1 (Boden *et al.*, 1999; Gehringer *et al.*, 2000; Yerly *et al.*, 1999).

Genotypic and phenotypic resistance testing are the two major ways to determine the drug resistance of clinical HIV-1 isolates. For genotyping, the HIV-1 genome isolated from the infected individuals is sequenced. This HIV-1 genome is than cross-referenced with a database and we are able to predict the drug resistance profile of HIV-1. However, it is impossible to predict the phenotype when we encounter a combination of mutations that has never been documented. This may raise a concern when a new drug is released in the market. Another problem in the genotyping is the presence of genotype-phenotype discordance (Parkin *et al.*, 2003; Sarmati *et al.*, 2002).

Alternatively, for the phenotypic resistance testing, the drug resistance profiles are measured by many biological/virological assay systems (Hertogs *et al.*, 1998; Iga *et al.*, 2002; Jarmy *et al.*, 2001; Kellam & Larder, 1994; Menzo *et al.*, 2000; Walter *et al.*, 1999). Phenotypic resistance testing is powerful because the diagnosis is based on experimental observations. Among the systems, ones that depend on the multi-round HIV-1 replication seemed to provide the best drug resistance data reflecting the *in vivo* condition. However, many drug-resistant mutants have lower replication capabilities than wild-type (wt) HIV-1, which makes the phenotypic resistance testing difficult and time-consuming. In order to overcome these problems, it would be useful to develop a technique to make HIV-1

replicate faster without altering the effectiveness of antiretroviral compounds.

During our search for an inhibitor of HIV-1 replication, we found sparsomycin, a metabolite from *Streptomyces sparsogenes*, which reproducibly enhanced the replication of HIV-1. Therefore, we tested whether sparsomycin merits phenotypic drug resistance profiling studies on low-fitness HIV-1 isolates.

Materials and methods

Cells and viruses

Human embryonic kidney (HEK) 293T cells were maintained in Dulbecco's modified Eagle's medium (Sigma-Aldrich, Tokyo, Japan) supplemented with 10% fetal bovine serum (FBS; Hyclone, Logan, UT, USA), penicillin and streptomycin (Invitrogen, Carlsbad, CA, USA). H9, Jurkat, SupT1 and HPB-Ma cells were maintained in RPMI1640 (Sigma-Aldrich) supplemented with 10% FBS, penicillin and streptomycin. All the cell lines were incubated at 37°C in a humidified 5% CO_2 atmosphere. As previously described, HIV-1 (HXB2) was produced by transfecting proviral DNA into 293T cells and collecting the culture medium 3 days post-transfection (Komano *et al.*, 2004). The replication-incompetent HIV-1 (HXB2 Δ*vpr*, Δ*rev*, Δ*env*, Δ*nef*) was produced by transfecting the proviral DNA carrying renilla luciferase with the *nef* open reading frame into 293T cells, along with the expression plasmid for *env*, *tat*, *rev* and *nef* (pIIIex) as described previously in Komano *et al.* (2004). As previously described, the D30N, L90M, and D25N protease mutants of HIV-1 were generated by the site-directed mutagenesis (Sugiura *et al.*, 2002). The multidrug-resistant HIV-1 DR3577 was a clinical isolate from a patient on HAART in which reverse transciptase carried the following mutations M41L, D67N, K70R, V75M, K101Q, T215F and K219Q, and protease carried the following mutations L10I, K20R, M36I, M46I, L63P, A71V, V82T, N88S and L90M. For the generation of replication-incompetent murine leukaemia virus (MLV) vector expressing firefly luciferase, pCMMP luciferase was transfecting into 293T cells along with *gag/pol* and VSV-G expressing plasmids as described previously (Komano *et al.*, 2004).

Chemical compound

Sparsomycin was either purchased from Sigma-Aldrich (cat. S1667) or obtained from Dr Nakajima (Toyama Prefectural University, Toyama, Japan). Sparsomycin was dissolved in 2mM dimethyl sulphoxide and stored at –20°C until use.

Monitoring HIV-1 replication

For HIV-1 infection, 1×10^6 cells were incubated with the culture supernatant containing approximately 10 ng of p24. Alternatively, wt HIV-1, or D30N and L90M mutants were introduced into cells either by electroporation or DEAE-dextran-mediated protocol as previously described (Matsuda *et al.*, 1993; Miyauchi *et al.*, 2005). The culture supernatants were collected everytime the infected cells were split until they ceased to proliferate. The amount of p24 antigen of HIV-1 in the culture supernatants was quantified by using Retro TEK p24 antigen ELISA kit according to the manufacturer's protocol (Zepto Metrix, Buffalo, NY, USA). The signal was detected by Vmax ELISA reader (Molecular Devices, Palo Alto, CA, USA).

Determining 50% inhibitory concentrations (IC_{50})

IC_{50} was calculated by using a reporter cell line, MARBLE, developed by Sugiura *et al.* (personal communication). In brief, a clone of HPB-Ma carrying the long terminal repeat (LTR)-driven firefly luciferase cassette integrated in its genome was infected with HIV-1 and incubated in the presence of varying concentrations of antiretroviral compounds for a week. The cells were then lysed to measure the firefly luciferase activity, which represented the propagation of HIV-1 in culture. The firefly luciferase activity was normalized by constitutively-expressed renilla luciferase activity. The dual luciferase assay was performed according to the manufacturer's protocol (Promega, Madison, WI, USA). Chemiluminescence was detected by Lmax (Molecular Devices).

Reporter assay

The –1 frameshift reporters, pLuc (–1) and pLuc (0), were kindly provided by Dr Brakier-Gingras (Dulude *et al.*, 2002). The renilla luciferase expression vector phRL/CMV was purchased from Promega. pLTR Luc encoded GFP-luciferase under the regulation of HIV-1's LTR promoter (Komano *et al.*, 2004). pLTRΔnefLuc encoded renilla luciferase by substituting *nef* in the proviral context of HXB2 (Komano *et al.*, 2004). Plasmids were transfected into 293T cells by Lipofectamine 2000 plus reagent in accordance with the manufacturers' protocol (Invitrogen). For the detection of luciferase activities, the dual glo luciferase assay was performed at 2–3 days post-transfection or post-infection according to the manufacturers' protocol (Promega). The signal was detected by Vmax ELISA reader (Molecular Devices).

Western blot analysis

COS-7 cells were transfected with Lipofectamine 2000 (Invitrogen) or Fugen6 (Roche, Basel, Switzerland) according to the manufacturer's protocol with proviral DNA encoding the D25N protease mutant. At 48 h post-transfection, cells were washed with PBS and lysed in a buffer containing 4% SDS, 100 mM Tris-HCl (pH 6.8), 12% 2-ME, 20% glycerol and bromophenol blue.

Samples were boiled for 10 min. Protein lysates approximately equivalent to 5×10^4 cells were separated in 5–20% SDS-PAGE (Perfect NT Gel, DRC, Tokyo, Japan), transferred to a polyvinylidene fluoride (PVDF) membrane (Immobilon-P^{SQ}; Millipore, Billerica, MA, USA), and blocked with 5% dried non-fat milk (Yuki-Jirushi, Tokyo, Japan) in PBS. For the primary antibody, we used rabbit anti-*Gag* polyclonal antibody or mouse anti-*Gag* monoclonal antibody. For the secondary antibody, either a biotinylated anti-rabbit antibody or a biotinylated anti-mouse goat antibody (GE Healthcare Bio-Science, Piscataway, NJ, USA) was used. For the tertiary probe, a horseradish peroxidase-conjugated streptoavidin (GE Healthcare Bio-Science) was used. Signals were developed by incubating blots with a chemilumenescent horseradish peroxidase substrate (GE Healthcare Bio-Science) and detected by using Lumi-Imager F1 (Roche).

Results

The structure of sparsomycin, a metabolite from *Streptomyces sparsogenes,* is unique in that it comprises two unusual entities, a monooxodithioacetal moiety and a uracil acrylic acid moiety (Figure 1A). H9 cells were infected with HIV-1 and then maintained in the presence of varying concentrations of sparsomycin. Dimethyl sulphoxide was added in the absence of sparsomycin throughout this study. At 7 days post-infection, a massive syncytial formation was found in the presence of sparsomycin (Figure 1B). The higher the concentration of sparsomycin, the faster p24 accumulated in the culture supernatants (Figure 1C). Similar observations were made in Jurkat, SupT1 (Figures 1D and E), and HPB-Ma cells although the speed of p24 accumulation appeared different among the cell lines. On the other hand, sparsomycin did not show any detectable effect on the cell growth under concentrations of 500 nM.

These results could be due to sparsomycin's ability to either boost HIV-1 replication or select a mutant that replicated substantially faster than the wt HIV-1. To differentiate these possibilities, we recovered the virus-containing culture supernatants from the H9 cell culture at the peak of HIV-1 replication in the presence of 400 nM sparsomycin (asterisk in Figure 1F). Then fresh H9 cells were infected with the recovered virus, the cells were split into two samples and 400 nM of sparsomycin was added to each sample. If sparsomycin selected fast-growing mutants, the replication profiles of HIV-1 should resemble the original sample with sparsomycin (solid circle, Figure 1F) regardless of sparsomycin's presence. However, the replication profile in the presence of sparsomycin shifted leftward (Figure 1G), suggesting that it was unlikely that sparsomycin selected the fast-replicating viral mutants. Therefore, it is likely that sparsomycin boosted HIV-1 replication. Replication-enhancing effects were also seen by using the chemically-synthesized derivatives of sparsomycin (unpublished data; Nakajima *et al.*, 2003). The replication-boosting effect levelled-out at 500 nM, an approximately 20-fold lower concentration than the 50% toxic dose (TD_{50}) of sparsomycin (Ash *et al.*, 1984).

To demonstrate the usefulness of sparsomycin in HIV-1 research, we have examined whether sparsomycin can also boost the replication of drug-resistant low-fitness isolates. The D30N and L90M are common drug-resistant mutations found within HIV-1 protease in HIV-1-infected patients on HAART (Devereux *et al.*, 2001; Kantor *et al.*, 2002; Pellegrin *et al.*, 2002; Sugiura *et al.*, 2002). We introduced proviral DNA carrying the D30N or L90M mutation into H9, Jurkat, and SupT1 cells. HIV-1 replication was than monitored in the presence of 400 nM of sparsomycin. The replication of both viral mutants was substantially enhanced in the presence of sparsomycin in H9 cells (Figures 2A and B). The replication of the L90M-carrying mutant was also enhanced in Jurkat and SupT1 cells (Figures 2C and D). Of note, the replication enhancement appeared profound when HIV-1 displayed relatively slower replication kinetics (for example, the replication of D30N-carrying mutant versus the wt HIV-1 in H9 cells or the replication of HIV-1 in SupT1 versus H9 cells).

Considering the use of sparsomycin in the phenotypic resistance testing, it is critical to know whether sparsomycin affects HIV-1's sensitivity to the antiretroviral drugs. The respective IC_{50} of representative antiretroviral drugs in the absence and the presence of 400 nM sparsomycin were as follows: reverse transcriptase inhibitors; lamivudine, 13.7 and 10.4 nM, and stavudine, 6.3 and 17.0 nM; an non-nucleoside reverse transcriptase inhibitor, nevirapine, 78.2 and 146.4 nM; and protease inhibitors, nelfinavir, 2.8 and 1.0 nM, indinavir, 4.2 and 3.0 nM, and amprenavir, 3.4 and 3.3 nM. Then, we examined whether the presence of sparsomycin affected the IC_{50} of both zidovudine (AZT) and lopinavir (LPV) against a multidrug-resistant HIV-1 isolate, DR3577. The magnitude of both AZT and LPV-resistance of DR3577 was in the order of 2 log (data not shown). The IC_{50}s of AZT in the presence and absence of 400 nM sparsomycin were 14.0 and 36.7 nM, respectively, and for LPV they were 103.1 and 78.9 nM, respectively. These data suggested that the presence of sparsomycin did not significantly influence the IC_{50} of antiretroviral drugs on the replication of both wt and drug-resistant HIV-1.

Finally, we investigated the possible mechanisms that sparsomycin enhanced the replication of HIV-1 and its mutants although the estimated magnitude of enhancement per single replication cycle was small. To do this, we used non-T cells to increase the sensitivity of assays. First, we examined if the early phase of HIV-1's life cycle was

Figure 1. The enhancement of HIV-1 replication by sparsomycin

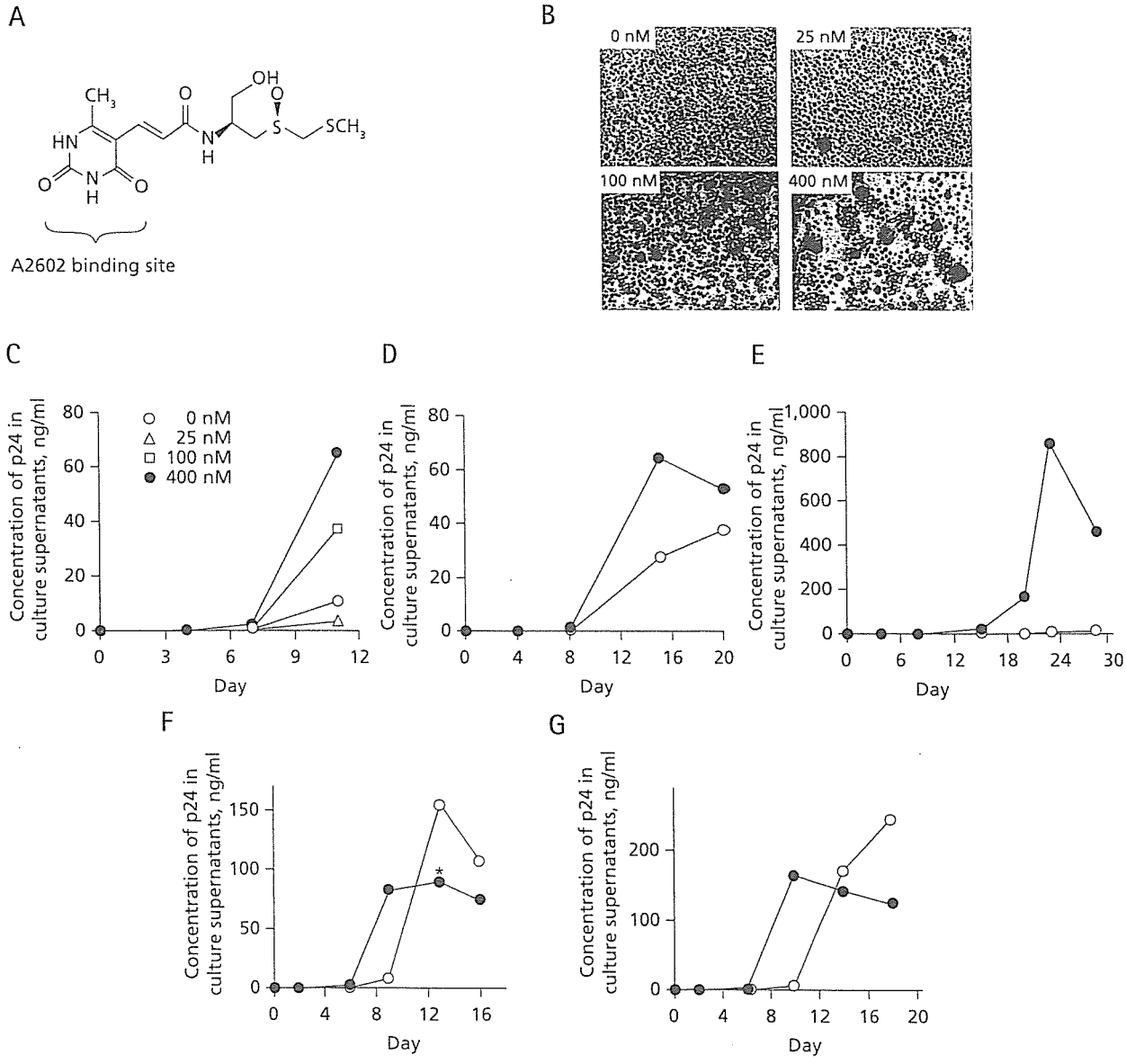

(A) Structure of sparsomycin. The uracil acrylic acid moiety confers the binding capacity to the conserved nucleobase A2602 of the large ribosomal subunit. **(B)** H9 cells infected with HIV-1 were photographed at a week after infection (magnification, ×200). **(C)** The replication profiles of HIV-1 in H9 cells in the presence of varying concentrations of sparsomycin. **(D-G)**. The replication profiles of HIV-1 in Jurkat **(D)**, SupT1 **(E)**, and H9 cells **(F and G)** in the presence of sparsomycin (400 nM, solid circle) or in the absence (open circle; **F and G**). Virus-containing culture supernatant was collected at 13 days post-infection (asterisk, F) to infect fresh H9 cells and the replication profiles of HIV-1 were analysed in the presence of sparsomycin (400 nM, solid circle) or in the absence (open circle, G).

positively affected by sparsomycin. In the presence of increasing concentrations of sparsomycin, 293 $CD4^+$ T-cells and NP2 CD4 CXCR4 cells were infected with either a replication-deficient HIV-1 vector enveloped with its own *Env* or a VSV-G-psueodotyped MLV vector. Two days post-infection, cells were lysed to measure the luciferase activities representing the efficiency of viral infection. Our results indicate that luciferase activities were not significantly increased at the replication-enhancing dose for both HIV-1 and MLV vectors (Figure 3A). Thus suggesting that the early phase of the retroviral life cycle was not detectably affected by sparsomycin.

Figure 2. Sparsomycin's ability to enhance replication of low-fitness drug resistant HIV-1 mutants

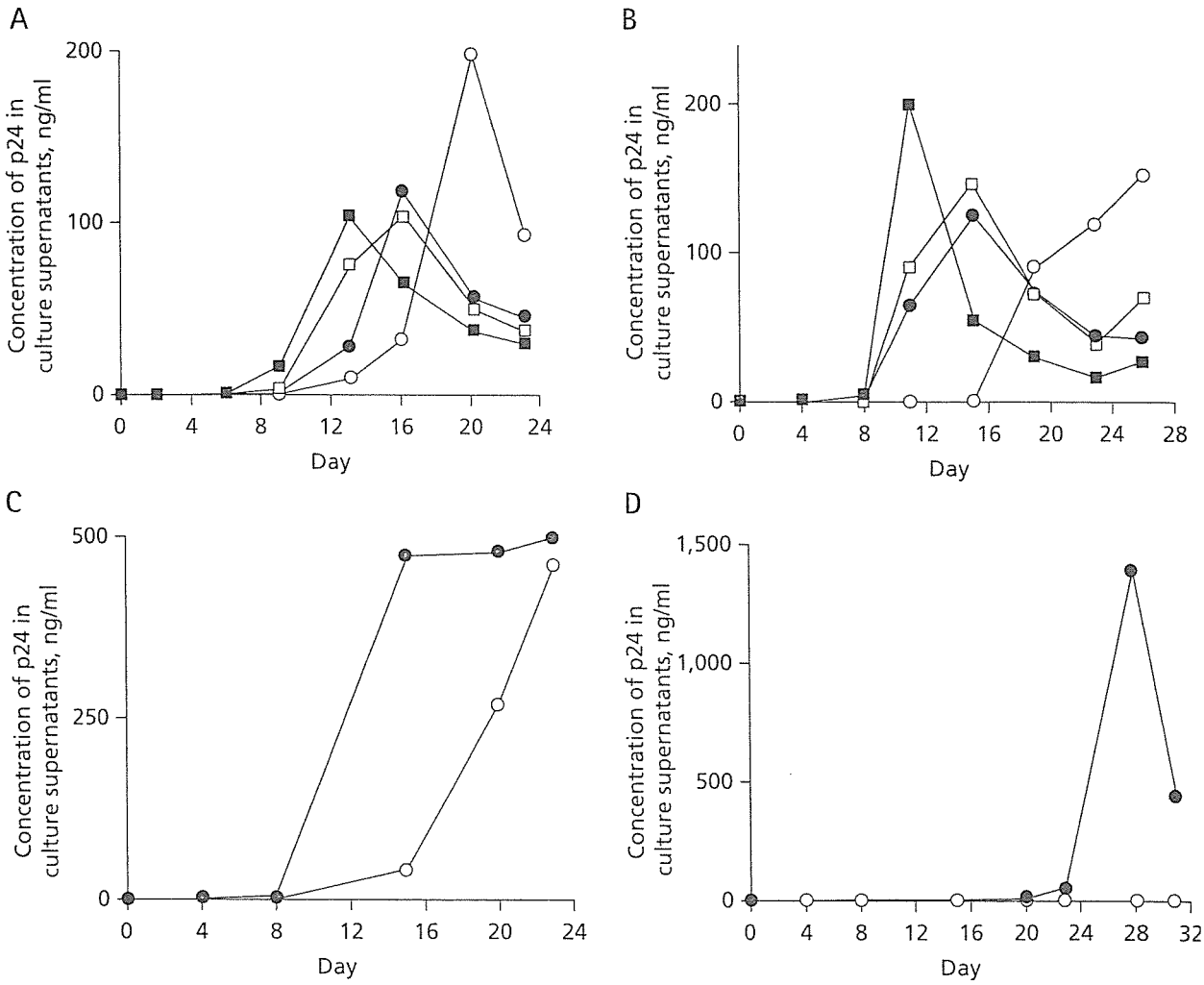

(A and B) The replication kinetics of the D30N-carrying (circle) and L90M-carrying (square) mutants in the presence of sparsomycin (400 nM, solid) or in the absence (open) were investigated twice independently in H9 cells. **(C and D)** The replication kinetics of the L90M-carrying mutant were examined in Jurkat cells **(C)** and SupT1 cells **(D)** in the presence of sparsomycin (400 nM, solid circle) or in the absence (open circle).

Next, we examined the possible active role of sparsomycin in the late phase of HIV-1's life cycle. Sparsomycin has been reported to be a potential enhancer of the −1 frameshift (Dinman *et al.*, 1997). Therefore, we tested whether sparsomycin could positively affect the efficiency of the translational −1 slip at HIV-1's frameshift signal using the reporter assay system established by Dulude *et al.* (2002). The −1 frameshift reporter was created by placing the firefly luciferase in the *pol* frame, pLuc(−1), whereas the control plasmid pLuc(0) has the luciferase in the *gag* frame after the frameshift signal (Figure 3B). In addition, HIV-1's LTR-driven luciferase reporter constructs were tested (pLTR Luc and pLTRΔnefLuc; Figure 3B). We transfected these reporter plasmids into 293T cells along with the renilla luciferase-expressing plasmid phRL/CMV (Promega) to measure the non-specific or toxic effects, if any, of sparsomycin. Cells were incubated in the presence of varying concentrations of sparsomycin for 3 days. Then the dual luciferase assay was performed. The pLuc(−1) behaved differently from the other groups in that the luciferase activities from the pLuc(−1) increased in a dose-dependent fashion. The magnitude of increasement was 2.3-fold at the replication-enhancing dose (Figure 3C). The positive correlation between the relative luciferase activity and the concentration of sparsomycin was statistically significant (r=0.926, P<0.001, n=8, Student's t-test). In contrast, the luciferase activities from the other reporters, even the renilla luciferase plasmid

co-transfected with the pLuc(-1) vector, remained unchanged (Figure 3C). These data suggested that sparsomycin positively affected the efficiency of HIV-1's –1 frameshift. It also suggested that sparsomycin did not enhance transcription from the viral promoter or the translation of proteins driven by the LTR promoter to enhance HIV-1 replication.

If the efficiency of –1 frameshift was increased, we would expect that the *Gag–Pol* to *Gag* ratio to increase. To test this, we transfected COS-7 cells with the HIV-1's proviral DNA carrying the D25N mutation in protease that produced catalytically inactive protease to increase the sensitivity of detecting *Gag–Pol* (Xie *et al.*, 1999). When sparsomycin was added, the intensities of *Gag–Pol* gradually increased in relation to the reporter assay. The *Gag–Pol* to *Gag* ratio reached 1.3-fold at 400 nM sparsomycin when normalized with results produced in the absence of sparsomycin (Figure 3D). The average and standard deviation of the *Gag–Pol* to *Gag* ratio from four independent experiments were 1.29 ± 0.14 at the replication enhancing concentration of sparsomycin (1.29-, 1.48-, 1.16-, and 1.24-fold increase). Similar results were obtained by using

Figure 3. The possible mechanism of HIV-1 replication enhancement by sparsomycin

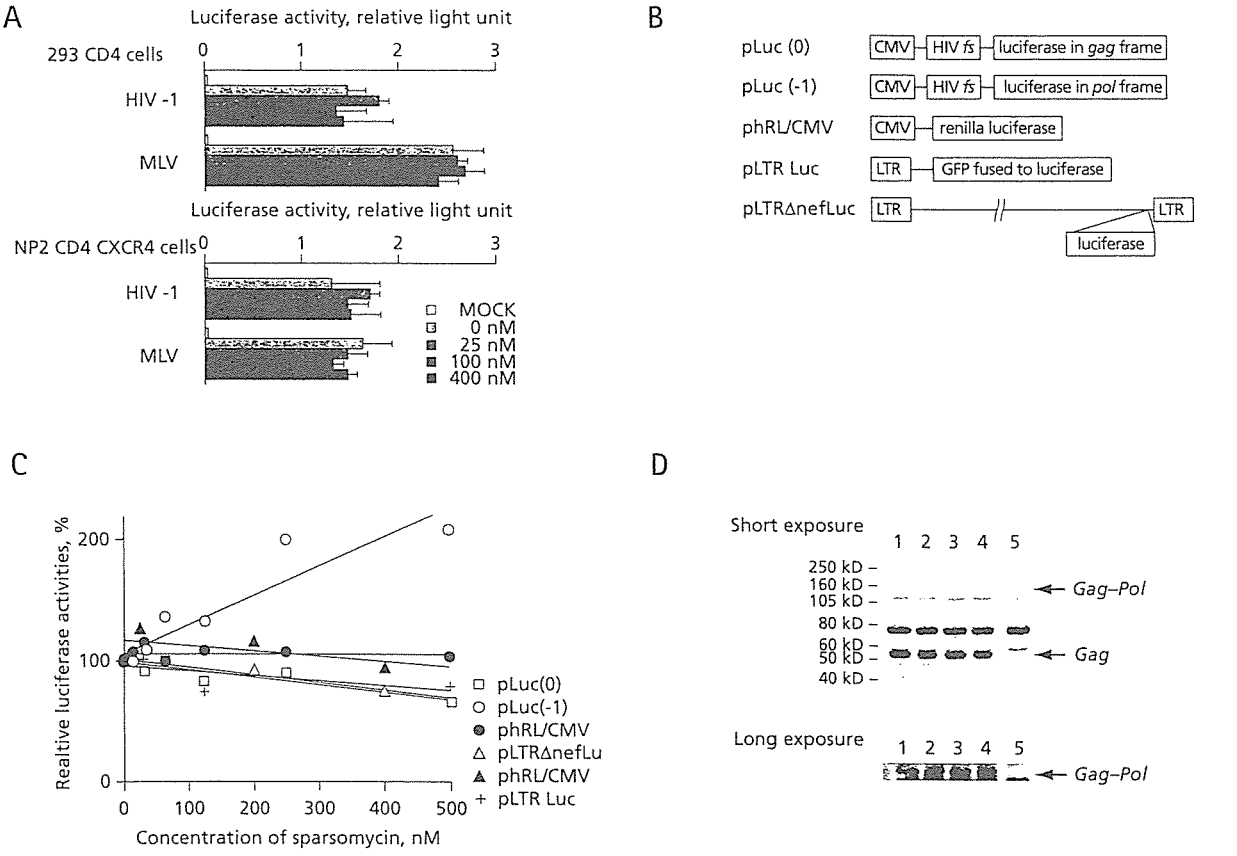

(A) The single round infection efficiencies of HIV-1 and murine lukaemia virus (MLV) vectors measured by the virally-encoded luciferase activities in 293 CD4⁺ T-cells and NP2 CD4 CXCR4 cells in the presence of varying concentrations of sparsomycin. (B) The schematic drawing of constructs used in the reporter assay. The HIV-1's frameshift signal (*fs*) was placed between the CMV promoter and the luciferase. The luciferase was placed in either the *gag* frame (pLuc(0)) or the *pol* frame (pLuc(-1)). The renilla luciferase expression vector phRL/CMV was used in parallel. The pLTR Luc encodes the GFP-luciferase driven by HIV-1's LTR promoter. The pLTRΔnefLuc has the renilla luciferase substituting *nef* in the proviral context of HXB2. (C) The luciferase activities from the above reporter constructs without sparsomycin were set as 100% and the relative luciferase activities in the presence of sparsomycin were shown. The renilla luciferase activities from phRL/CMV were shown for the pLuc(-1) (solid circle) and pLTRΔnefLuc (solid triangle) transfections in particular. The pLuc(-1) behaved differently from the other groups and the positive correlation between the relative luciferase activity and the concentration of sparsomycin was statistically significant (r=0.926, P<0.001, n=8, Student's t-test). The SD was within 10% from the avgerage. Shown are the representative data from two independent experiments. (D) Western blot analysis to measure the *Gag–Pol* and *Gag* ratio. Cell extracts were separated in the SDS-polyacrylamide gel and immunoblotted by using the rabbit polyclonal antibodies raised against p24. (lane 1, 0 nM; lane 2, 20 nM; lane 3, 200 nM; lane 4, 400 nM; lane 5, MOCK). The lower panel shows the *Gag–Pol* signal obtained from the long exposure of the same blot.